HOKKAIDO UNIVERSITY

Title	Configuration of propagator method for calculation of electron velocity distribution function in gas under crossed electric and magnetic fields
Author(s)	SUGAWARA, Hirotake
Citation	Plasma Science and Technology, 21(9), 094001-1-094001-18 https://doi.org/10.1088/2058-6272/ab20e0
Issue Date	2019-06-21
Doc URL	http://hdl.handle.net/2115/78664
Rights	This is a peer-reviewed, un-copyedited version of an article accepted for publication/published in Plasma Sources Science and Technology. IOP Publishing Ltd is not responsible for any errors or omissions in this version of the manuscript or any version derived from it. The Version of Record is available online at 10.1088/2058-6272/ab20e0. This Accepted Manuscript is available for reuse under a CC BY-NC-ND 3.0 licence after the 12 month embargo period provided that all the terms of the licence are adhered to.
Rights(URL)	https://creativecommons.org/licenses/by-nc-nd/3.0/
Type	article (author version)
File Information	Sugawara02-2019-PST-HUSCAP.pdf

Instructions for use

Hokkaido University Collection of Scholarly and Academic Papers : HUSCAP

Configuration of propagator method for calculation of electron velocity distribution function in gas under crossed electric and magnetic fields ‡

Hirotake Sugawara

Division of Electronics for Informatics, Graduate School of Information Science and Technology, Hokkaido University, Sapporo 060-0814, Japan

E-mail: sugawara@ist.hokudai.ac.jp

Abstract. This paper presents a self-contained description on the configuration of propagator method (PM) to calculate the electron velocity distribution function (EVDF) of electron swarms in gases under dc electric and magnetic fields crossed at a right angle. Velocity space is divided into cells with respect to three polar coordinates v, θ and ϕ. The number of electrons in each cell is stored in three-dimensional arrays. The changes of electron velocity due to acceleration by the electric and magnetic fields and scattering by gas molecules are treated as intercellular electron transfers on the basis of the Boltzmann equation and are represented using operators called the propagators or Green's functions. The collision propagator, assuming isotropic scattering, is basically unchanged from conventional PMs performed under electric fields without magnetic fields. On the other hand, the acceleration propagator is customized for rotational acceleration under the action of the Lorentz force. The acceleration propagator specific to the present cell configuration is analytically derived. The mean electron energy and average electron velocity vector in a model gas and SF_6 were derived from the EVDF as a demonstration of the PM under the Hall deflection and they were in a fine agreement with those obtained by Monte Carlo simulations. A strategy for fast relaxation is discussed, and extension of the PM for the EVDF under ac electric and dc/ac magnetic fields is outlined as well.

‡ Published source: Plasma Science and Technology, vol. 21, no. 9, 094001 (18 pages) (2019)
DOI: 10.1088/2058-6272/ab20e0

1. Introduction

Calculation of the electron velocity/energy distribution function (EVDF/EEDF) is one of the most fundamental bases for evaluation of the electron transport and reactions in electrical discharges and plasmas. Boltzmann equation (BE) analyses are a typical approach to the EVDF. However, their formulation includes technical mathematics such as a series expansion of the EVDF using orthogonal functions [1, 2, 3, 4], and some advanced efforts using a multi-term BE analysis varied even the number of expansion terms as a parameter to confirm the convergence of the solutions of anisotropic or distorted EVDFs [5, 6, 7]. Practical composition of such a BE analysis code would require highly sophisticated experience in operating more or less abstract simultaneous differential equations. In contrast, Monte Carlo (MC) simulations to treat electron behavior on the basis of a particle model are of a clear picture. Instead, MC simulations require a heavy computational load to track a huge number of samples to reduce statistical fluctuation due to use of random numbers. Nevertheless, it is not easy to judge the convergence of the EVDF under relaxation with fluctuation nor to estimate *ab initio* a sufficient relaxation time to reach equilibrium.

The propagator method (PM), detailed in this paper, is a numerical technique to solve the BE more directly than using the series expansion. Velocity space is divided into cells, the EVDF is represented by the number of electrons in each cell, and the intercellular electron transfers due to electron acceleration and collisions are quantified using operators called the propagators or Green's functions. Starting from a given initial EVDF, relaxation of the EVDF to its equilibrium solution is calculated by repeatedly applying the propagators to the EVDF. The PM requires huge arrays to store the number of electrons and cell properties. Instead, physical aspects of the electron motions in velocity space are kept as are in a particle model. Furthermore, the PM is considered to be suitable for parallel computing because the PM is carried out mainly with multiply-add operations.

The PM have been applied mostly to the EVDFs/EEDFs under electric fields $\mathbf{E}$ without magnetic field $\mathbf{B}$. Some examples are for time-dependent EVDFs under dc $\mathbf{E}$ [8, 9], those under radio-frequency $\mathbf{E}$ [10, 11, 12], and impulse $\mathbf{E}$ [13], equilibrium and non-equilibrium EEDFs in the steady-state Townsend modes [14, 15, 16, 17], analyses of drift velocities [18], derivation of longitudinal and transverse diffusion coefficients

[19, 20, 21], etc. Furthermore, the PM has been extensively applied to objects other than electrons; ion transport [22], excited species, and radiation [23, 24, 25, 26, 27], and carrier in semiconductor [28]. A brief history of the PM was presented in recent papers [29, 30].

Under $\mathbf{E}$ without $\mathbf{B}$, we can assume a rotational symmetry of the EVDF around the axis in the direction of $\mathbf{E}$. The EVDF becomes a two-variable function, thus it can be calculated with two-dimensional (2D) arrays. On the other hand, in the presence of $\mathbf{B}$, we need three-dimensional (3D) arrays to deal with the EVDF no longer axisymmetric under the action of the Lorentz force. The cost for the memory capacity and computational time had limited the PM calculations under crossed $\mathbf{E}$ and $\mathbf{B}$ in early decades. However, recent enriched computational resources have enabled us to perform the 3D PM calculations with ordinary workstations [30, 31, 32, 33, 34]. This would contribute to analyses of fundamental properties of magnetized plasmas.

In this paper, ever unwritten details of the PM calculation for the EVDF under $\mathbf{E}$ and $\mathbf{B}$ crossed at a right angle ($\mathbf{E} \times \mathbf{B}$ fields) are described as necessary specification in composition of a PM program. This field configuration $\mathbf{E} \perp \mathbf{B}$ is applicable for whole space in chambers for characteristic inductively coupled magnetized plasmas so-called neutral loop discharge plasmas for etching [35, 36, 37, 38, 39] and X-point plasmas for ion source [40, 41, 42, 43, 44]. The consideration of the Lorentz force requires not only an extension of the arrays from 2D ones to 3D ones but also the change of the electron acceleration field in velocity space from translational one to rotational one, and a modification of the numerical scheme accompanies. In a chosen cell configuration under these substantial changes, an analytical derivation of the propagator for electron acceleration is presented as a key component of the PM. The validity of the numerical scheme is shown in comparisons of electron transport parameters and the EVDF with those obtained by a BE analysis and MC simulations. An effort pursuing faster relaxation is also made.

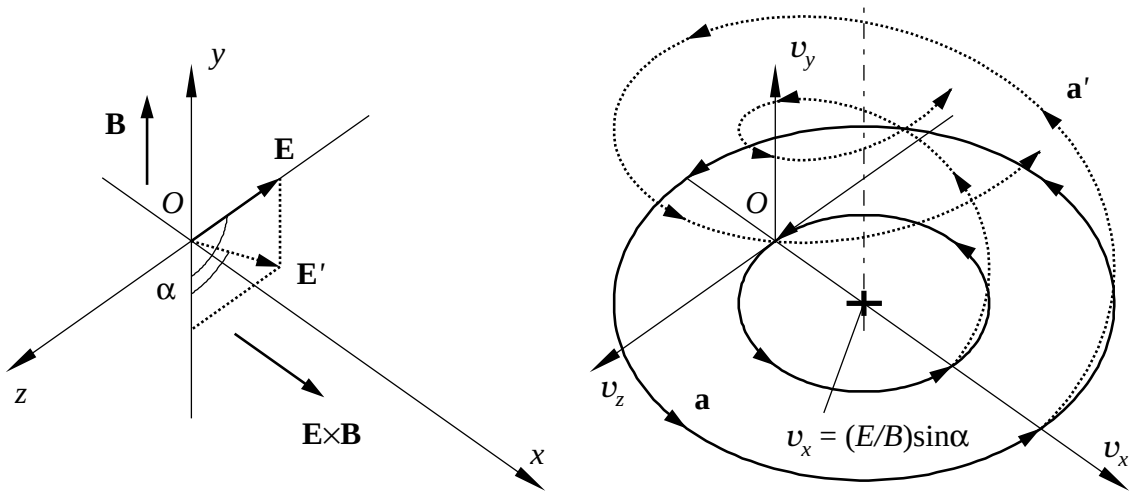

Figure 1. Coordinate system (x, y, z), applied electric and magnetic fields $\mathbf{E}$ and $\mathbf{B}$, and acceleration vector $\mathbf{a} = -(e/m)(\mathbf{E} + \mathbf{v} \times \mathbf{B})$ in velocity space (v_x, v_y, v_z). $\mathbf{a}$ and $\mathbf{a}'$ correspond to $\mathbf{E}$ and $\mathbf{E}'$, respectively.

2. Simulation model

2.1. Electron motion in electric and magnetic fields

In boundary-free real space $\mathbf{r} = (x, y, z)$, $\mathbf{E}$ and $\mathbf{B}$ are defined as follows:

$$\mathbf{E} = (E_x, E_y, E_z) = (0, -E\cos\alpha, -E\sin\alpha), \tag{1}$$

$$\mathbf{B} = (B_x, B_y, B_z) = (0, B, 0), \tag{2}$$

where $E > 0$, $B > 0$, and α is the angle between $\mathbf{E}$ and $-\mathbf{B}$ as shown in figure 1.

The electron velocity $\mathbf{v}$ is written with both Cartesian coordinates v_x, v_y and v_z and polar coordinates v, θ and ϕ as

$$\mathbf{v} = (v_x, v_y, v_z) = (v\sin\theta\cos\phi, v\cos\theta, v\sin\theta\sin\phi), \tag{3}$$

where $v = |\mathbf{v}|$, θ is the polar angle between the v_y-axis and $\mathbf{v}$ vector, and ϕ is the azimuthal angle around the v_y-axis. The Cartesian coordinates v_x, v_y and v_z are used mainly for description of the electron motion, and the polar coordinates v, θ and ϕ are for the cell configuration detailed in section 3.2.

The electron flow in velocity space is governed by the electron acceleration $\mathbf{a} = (a_x, a_y, a_z)$ under the Coulomb and Lorentz forces. The electron motion equation is

written as

$$\mathbf{a} = \frac{\mathrm{d}}{\mathrm{d}t}\mathbf{v} = -\frac{e}{m}(\mathbf{E}+\mathbf{v}\times\mathbf{B}), \tag{4}$$

$$a_x = \frac{\mathrm{d}}{\mathrm{d}t}v_x = \frac{e}{m}v_z B = \omega v_z, \tag{5}$$

$$a_y = \frac{\mathrm{d}}{\mathrm{d}t}v_y = \frac{e}{m}E\cos\alpha = \omega\frac{E}{B}\cos\alpha, \tag{6}$$

$$a_z = \frac{\mathrm{d}}{\mathrm{d}t}v_z = \frac{e}{m}(-v_x B + E\sin\alpha) = -\omega\left(v_x - \frac{E}{B}\sin\alpha\right), \tag{7}$$

where e and m are the electronic charge and mass, and $\omega = eB/m$ is the electron cyclotron angular frequency. The projection of an electron free-flight locus in velocity space on the $v_x v_z$-plane is a circle centered at $(v_x, v_z) = ((E/B)\sin\alpha, 0)$ [30, 45] because

$$\left(v_x - \frac{E}{B}\sin\alpha\right)^2 + v_z^2 = \left(v_x|_{t=0} - \frac{E}{B}\sin\alpha\right)^2 + (v_z|_{t=0})^2. \tag{8}$$

$(E/B)\sin\alpha$ is the $\mathbf{E}\times\mathbf{B}$ drift velocity in the x direction under collision-less condition. $\mathbf{a}$ is parallel to the $v_x v_z$-plane when $\alpha = \frac{1}{2}\pi$ (i.e. $\mathbf{E}\perp\mathbf{B}$). Otherwise, the electron motion in velocity space is helical around the axis passing the center of the circle in parallel to the v_y-axis. An overview is depicted in figure 1. Hereafter, we assume $\mathbf{E}\perp\mathbf{B}$.

2.2. Collisional processes

Binary collisions between electrons and gas molecules are considered in the present work, assuming the cold gas model and isotropic scattering in laboratory system. The collision frequency ν of a specific collisional process is given as $\nu = Nq(v)v$, where N is the gas molecule number density and q is the electron collision cross section of a gas molecule. The collisions are categorized into elastic momentum transfer, excitation, ionization and electron attachment. Let us denote the related quantities with subscripts 'mom', 'exc', 'ion' and 'att', respectively, in the description of the propagator for collisions.

3. Calculation scheme of propagator method

In the PM, the cells are defined by partitioning velocity space, an initial EVDF is given by distributing electrons to the cells, and the number of electrons in each cell in equilibrium is obtained by a relaxation scheme to satisfy simultaneous balance equations for the electron inflow and outflow represented using the acceleration and collision propagators. The present PM calculation follows the principle summarized in Ref.

[29, 30]. In this section, the cell configuration and the PM scheme are detailed from a viewpoint of practical coding.

3.1. Correspondence between the BE and the PM

The EVDF of an electron swarm is defined as $f(\mathbf{v}, t) = f(v_x, v_y, v_z, t)$. The EVDF in this form can be applied to spatially uniform electron distributions or the case that the positions of individual electrons are not cared. The BE for the EVDF is

$$\frac{\partial}{\partial t} f(\mathbf{v}, t) = \left[-\mathbf{a} \cdot \frac{\partial}{\partial \mathbf{v}} + \left(\frac{\partial}{\partial t} \right)_{\text{coll}} \right] f(\mathbf{v}, t). \tag{9}$$

$(\partial/\partial t)_{\text{coll}}$ is the collision operator representing the changes of electron velocity and population due to the collisional processes. Using the acceleration and collision propagators, $P_{\text{acc}}(\mathrm{d}\mathbf{v} \leftarrow \mathrm{d}\mathbf{v}')$ and $P_{\text{coll}}(\mathrm{d}\mathbf{v} \leftarrow \mathrm{d}\mathbf{v}')$, representing the electron transfers from a region $\mathrm{d}\mathbf{v}'$ to another $\mathrm{d}\mathbf{v}$ in velocity space, the BE can be rewritten as

$$\begin{aligned} &\frac{\partial}{\partial t} f(\mathbf{v}, t) \mathrm{d}\mathbf{v} \\ &\quad = \int_{\mathbf{v}' \neq \mathbf{v}} P_{\text{acc}}(\mathrm{d}\mathbf{v} \leftarrow \mathrm{d}\mathbf{v}') f(\mathbf{v}', t) \mathrm{d}\mathbf{v}' - \int_{\mathbf{v}' \neq \mathbf{v}} P_{\text{acc}}(\mathrm{d}\mathbf{v}' \leftarrow \mathrm{d}\mathbf{v}) f(\mathbf{v}, t) \mathrm{d}\mathbf{v} \\ &\quad + \int_{\mathbf{v}' \neq \mathbf{v}} P_{\text{coll}}(\mathrm{d}\mathbf{v} \leftarrow \mathrm{d}\mathbf{v}') f(\mathbf{v}', t) \mathrm{d}\mathbf{v}' - \int_{\mathbf{v}' \neq \mathbf{v}} P_{\text{coll}}(\mathrm{d}\mathbf{v}' \leftarrow \mathrm{d}\mathbf{v}) f(\mathbf{v}, t) \mathrm{d}\mathbf{v}. \end{aligned} \tag{10}$$

The positive and negative terms in the right-hand side represent, respectively, the electron inflow to and outflow from $\mathrm{d}\mathbf{v}$ due to collision and acceleration. Treatment of the collisions is described in section 3.5. That of the acceleration represented by $\mathbf{a} \cdot (\partial/\partial \mathbf{v})$ in the BE is detailed in section 3.6.

3.2. Cells

Three polar coordinates v, θ and ϕ are divided into sections for every $\Delta\varepsilon = \varepsilon_{\max}/i_{\max}$, $\Delta\theta = \pi/j_{\max}$ and $\Delta\phi = 2\pi/k_{\max}$, respectively, as shown in figure 2. Here, $\varepsilon = \frac{1}{2} m v^2$ is the electron energy. The (i, j, k)th cell $C_{i,j,k}$ is defined as the following region:

$$C_{i,j,k} : \ v_{i-1} \leq v \leq v_i, \ \theta_{j-1} \leq \theta \leq \theta_j, \ \phi_{k-1} \leq \phi \leq \phi_k, \tag{11}$$

where $v_i = v_{1\text{eV}} \sqrt{\varepsilon_i / \varepsilon_{1\text{eV}}}$, $\varepsilon_i = i\Delta\varepsilon$, $v_{1\text{eV}}$ is the electron speed associated with 1 eV, $\varepsilon_{1\text{eV}} = \frac{1}{2} m v_{1\text{eV}}^2 = 1\,\text{eV}$, $\theta_j = j\Delta\theta$ and $\phi_k = k\Delta\phi$. The volume $V_{i,j,k}$ of $C_{i,j,k}$ is

$$V_{i,j,k} = \int_{v_{i-1}}^{v_i} \int_{\theta_{j-1}}^{\theta_j} \int_{\phi_{k-1}}^{\phi_k} v^2 \sin\theta \, \mathrm{d}v \mathrm{d}\theta \mathrm{d}\phi = \frac{1}{3} (v_i^3 - v_{i-1}^3)(\cos\theta_{j-1} - \cos\theta_j) \Delta\phi. \tag{12}$$

The indices i, j and k range $1 \leq i \leq i_{\max}$, $1 \leq j \leq j_{\max}$ and $1 \leq k \leq k_{\max}$, respectively. It is convenient to set $j_{\max}$ to be an even integer and $k_{\max}$ to be a multiple

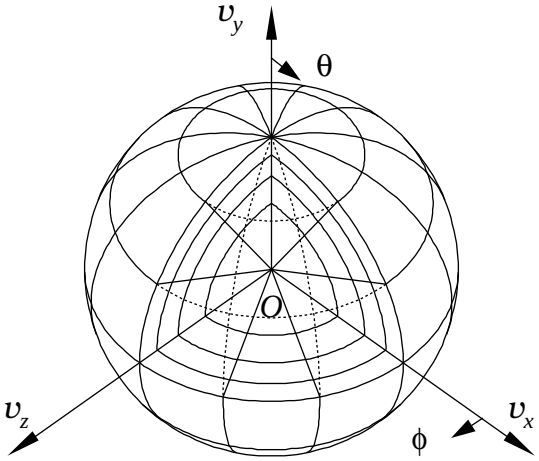

Figure 2. Cells defined in velocity space. Those in the octant of $v_x \geq 0$, $v_y \geq 0$ and $v_z \geq 0$ are omitted to show inner cells.

of four so that the v_xv_y-, v_xv_z- and v_yv_z-planes become cell boundaries. The parameters for the cell division, $\varepsilon_{\max}$, $i_{\max}$, $j_{\max}$ and $k_{\max}$, are empirically chosen to have sufficient extent and resolution to represent the EVDF. For example, we may choose $\varepsilon_{\max}$ and $i_{\max}$ so that the high-energy tail of the EEDF $F(\varepsilon_{\max})$ is sufficiently small and $\Delta\varepsilon$ is satisfactorily fine to discretize the thresholds of inelastic collisions.

Note here that these cells are concentric around the origin O of velocity space while the rotation center of $\mathbf{a}$ is shifted from O. This configuration makes the evaluation of the acceleration propagator partly irregular, but makes the treatment of isotropic scattering simple.

Let us denote the number of electrons in $C_{i,j,k}$ as $n_{i,j,k}$. A 3D array with a size of $i_{\max} \times \frac{1}{2}j_{\max} \times k_{\max}$ is necessary to store $n_{i,j,k}$. Here, reflectional symmetry of the EVDF with respect to the v_xv_z-plane, $f(v_x, v_y, v_z, t) = f(v_x, -v_y, v_z, t)$, is assumed because $\mathbf{E} \perp \mathbf{B}$. $n_{i,j,k}$ for $\frac{1}{2}j_{\max} + 1 \leq j \leq j_{\max}$ (i.e. $v_y \leq 0$) can be omitted to save the required memory capacity. Using $n_{i,j,k}$, the normalized EVDF $f(v)$ and EEDF $F(\varepsilon)$ are represented as

$$f(v_i^{\mathrm{R}})\frac{\Delta\varepsilon}{mv_i^{\mathrm{R}}} = F(\varepsilon_i^{\mathrm{R}})\Delta\varepsilon = \frac{1}{N_{\mathrm{e}}}\sum_{j=1}^{j_{\max}/2}\sum_{k=1}^{k_{\max}} n_{i,j,k}, \tag{13}$$

$$N_{\mathrm{e}} = \int_{v_x=-\infty}^{\infty}\int_{v_y=-\infty}^{\infty}\int_{v_z=-\infty}^{\infty} f(v_x, v_y, v_z)\,\mathrm{d}v_x\mathrm{d}v_y\mathrm{d}v_z = \sum_{i=1}^{i_{\max}}\sum_{j=1}^{j_{\max}/2}\sum_{k=1}^{k_{\max}} n_{i,j,k}, \tag{14}$$

where v_i^{R} and $\varepsilon_i^{\mathrm{R}}$ are the representative electron speed and energy of $C_{i,j,k}$ to plot the EVDF/EEDF, respectively, $\varepsilon_i^{\mathrm{R}} = (i - \frac{1}{2})\Delta\varepsilon = \frac{1}{2}m(v_i^{\mathrm{R}})^2$, and N_{e} is the total electron population. v_i^{R} and $\varepsilon_i^{\mathrm{R}}$ are referred to afterward for calculation of electron transport parameters.

In practical coding of the PM program, more 3D arrays of the same size as for $n_{i,j,k}$ are used to store the cell properties to quantify the acceleration propagator (section 3.6), because the cell properties are constants and referred to repeatedly in the PM calculation (section 3.7). The 3D arrays are prepared to have extra elements as margins outside of the calculation range; the zeroth and the $(i_{\max} + 1)$th elements for v, and those similar for θ and ϕ as well. This is because the calculation of $n_{i,j,k}$ refers to its neighbors $n_{i\pm1,j,k}$, $n_{i,j\pm1,k}$ and $n_{i,j,k\pm1}$. With the margin cells, the formulation can be regulated into a common form avoiding special treatments at the upper and lower ends of the index ranges. Here, because the series of cells indexed by k for ϕ are cyclic, the margin cells are equivalent to the cells on the opposite ends; i.e. $C_{i,j,0} = C_{i,j,k_{\max}}$ and $C_{i,j,k_{\max}+1} = C_{i,j,1}$. The properties of $C_{i,j,k_{\max}}$ and $C_{i,j,1}$ are copied to $C_{i,j,0}$ and $C_{i,j,k_{\max}+1}$, respectively, before the calculation of $n_{i,j,k}$, and those of $C_{0,j,k}$, $C_{i_{\max}+1,j,k}$, $C_{i,0,k}$ and $C_{i,j_{\max}/2+1,k}$ are set to be zero.

3.3. Cell boundaries

Let us define the cell boundaries as follows (see also figure 3). A v-boundary $B^v_{i,j,k}$ is the boundary between $C_{i,j,k}$ and $C_{i+1,j,k}$. $B^v_{i,j,k}$ is a part of a sphere centered at O;

$$B^v_{i,j,k} : \ v = v_i, \ \theta_{j-1} \le \theta \le \theta_j, \ \phi_{k-1} \le \phi \le \phi_k. \tag{15}$$

A θ-boundary $B^\theta_{i,j,k}$ is the boundary between $C_{i,j,k}$ and $C_{i,j+1,k}$. $B^\theta_{i,j,k}$ is a part of a cone whose apex is at O;

$$B^\theta_{i,j,k} : \ v_{i-1} \le v \le v_i, \ \theta = \theta_j, \ \phi_{k-1} \le \phi \le \phi_k. \tag{16}$$

A ϕ-boundary $B^\phi_{i,j,k}$ is the boundary between $C_{i,j,k}$ and $C_{i,j,k+1}$. $B^\phi_{i,j,k}$ is a part of a plane including the v_y-axis;

$$B^\phi_{i,j,k} : \ v_{i-1} \le v \le v_i, \ \theta_{j-1} \le \theta \le \theta_j, \ \phi = \phi_k. \tag{17}$$

Here, $B^\phi_{i,j,0} = B^\phi_{i,j,k_{\max}}$ is the boundary between $C_{i,j,k_{\max}}$ and $C_{i,j,1}$, because the series of cells indexed by k are cyclic.

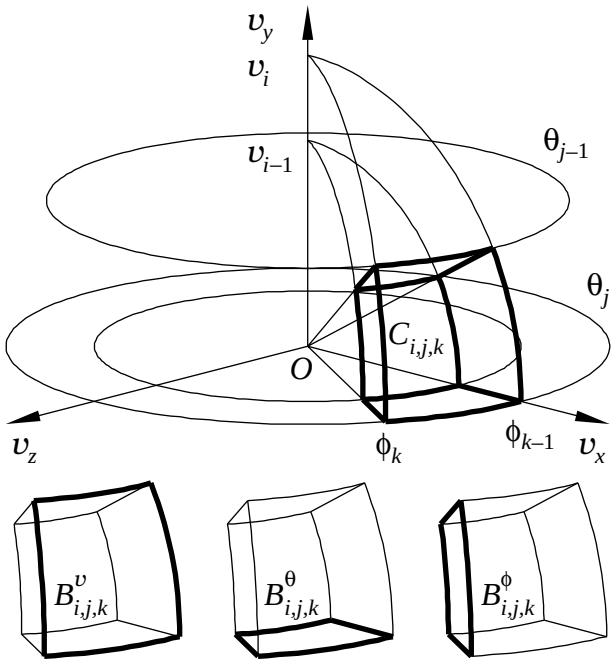

Figure 3. Cell $C_{i,j,k}$ and its boundaries $B^v_{i,j,k}$ ($v = v_i$), $B^\theta_{i,j,k}$ ($\theta = \theta_j$) and $B^\phi_{i,j,k}$ ($\phi = \phi_k$) facing to the $+v$, $+\theta$ and $+\phi$ directions, respectively.

$C_{i,j,k}$ has six boundaries $B^v_{i-1,j,k}$, $B^v_{i,j,k}$, $B^\theta_{i,j-1,k}$, $B^\theta_{i,j,k}$, $B^\phi_{i,j,k-1}$ and $B^\phi_{i,j,k}$. $B^v_{i,j,k}$ and $B^\theta_{i,j,k}$ are concentric boundaries, and $B^\phi_{i,j,k}$ represents radial boundaries. However, $B^v_{0,j,k}$ are degenerate at a point O, and $B^\theta_{i,0,k}$ and $B^\theta_{i,j_{\max},k}$ are lines on the v_y-axis. The electron outflows from $C_{i,j,k}$ through its boundaries are calculated in section 3.6 and Appendix.

3.4. The Boltzmann equation in equilibrium

The BE in equation (9) and its translation into the PM in equation (10) can be rewritten with inflow and outflow terms as follows [29, 30]:

$$\frac{\partial}{\partial t} f(\mathbf{v}, t) \mathrm{d}\mathbf{v} = \left[\left(\frac{\partial}{\partial t} \right)^{\mathrm{in}}_{\mathrm{acc}} - \left(\frac{\partial}{\partial t} \right)^{\mathrm{out}}_{\mathrm{acc}} + \left(\frac{\partial}{\partial t} \right)^{\mathrm{in}}_{\mathrm{coll}} - \left(\frac{\partial}{\partial t} \right)^{\mathrm{out}}_{\mathrm{coll}} \right] f(\mathbf{v}, t) \mathrm{d}\mathbf{v}. \tag{18}$$

In equilibrium, the EVDF is unchanged when normalized, but grows exponentially in the electron population as $(\partial/\partial t) f(\mathbf{v}, t) = \bar{\nu}_{\mathrm{ion}} f(\mathbf{v}, t)$, where $\bar{\nu}_{\mathrm{ion}} = \nu_{\mathrm{ion}} - \nu_{\mathrm{att}}$ is the effective ionization frequency. For discretized cells, equation (18) becomes

$$\left[\bar{\nu}_{\mathrm{ion}} + \left(\frac{\partial}{\partial t} \right)^{\mathrm{out}}_{\mathrm{acc}} + \left(\frac{\partial}{\partial t} \right)^{\mathrm{out}}_{\mathrm{coll}} \right] n_{i,j,k} = \left[\left(\frac{\partial}{\partial t} \right)^{\mathrm{in}}_{\mathrm{acc}} + \left(\frac{\partial}{\partial t} \right)^{\mathrm{in}}_{\mathrm{coll}} \right] n_{i,j,k}. \tag{19}$$

The inflow and outflow terms for a cell $C_{i,j,k}$ are given as follows:

$$\left(\frac{\partial}{\partial t}\right)^{\text{in}}_{\text{acc}} n_{i,j,k} = \sum_{i',j',k'} P_{\text{acc}}(C_{i,j,k} \leftarrow C_{i',j',k'}) n_{i',j',k'}, \tag{20}$$

$$\left(\frac{\partial}{\partial t}\right)^{\text{in}}_{\text{coll}} n_{i,j,k} = \sum_{i',j',k'} P_{\text{coll}}(C_{i,j,k} \leftarrow C_{i',j',k'}) n_{i',j',k'}, \tag{21}$$

$$\left(\frac{\partial}{\partial t}\right)^{\text{out}}_{\text{acc}} n_{i,j,k} = \sum_{i',j',k'} P_{\text{acc}}(C_{i',j',k'} \leftarrow C_{i,j,k}) n_{i,j,k}, \tag{22}$$

$$\left(\frac{\partial}{\partial t}\right)^{\text{out}}_{\text{coll}} n_{i,j,k} = \nu_{\text{total}} n_{i,j,k}, \tag{23}$$

where $\nu_{\text{total}} = N q_{\text{total}}(v_i^{\text{R}}) v_i^{\text{R}}$ is the total collision frequency, and q_{total} is the total collision cross section of a gas molecule. $P_{\text{acc}}(C_{i',j',k'} \leftarrow C_{i,j,k})$ and $P_{\text{coll}}(C_{i',j',k'} \leftarrow C_{i,j,k})$ represent the rates of electron transfer (ratio per unit time) from $C_{i,j,k}$ to $C_{i',j',k'}$ due to acceleration and collision, respectively. From equations (19)–(23), the condition that $n_{i,j,k}$ satisfies in the equilibrium (time-independent) solution of the EVDF is obtained as

$$n_{i,j,k} = \frac{\sum_{i',j',k'} \left[P_{\text{acc}}(C_{i,j,k} \leftarrow C_{i',j',k'}) + P_{\text{coll}}(C_{i,j,k} \leftarrow C_{i',j',k'})\right] n_{i',j',k'}}{\bar{\nu}_{\text{ion}} + \sum_{i',j',k'} P_{\text{acc}}(C_{i',j',k'} \leftarrow C_{i,j,k}) + \nu_{\text{total}}}. \tag{24}$$

This equation is used for the relaxation of the EVDF [29, 30]. P_{coll} and P_{acc} are quantified in sections 3.5 and 3.6, respectively. The relaxation scheme is explained in section 3.7.

3.5. Collision propagator

The collision propagator in the presence of $\mathbf{B}$ is basically unchanged from the conventional PM under $\mathbf{E}$ only [29]. It represents the changes of v, θ and ϕ occurring at scattering, and may include the change of electron population due to ionization and electron attachment. The rate of electron outflow from $C_{i,j,k}$ by collisions is quantified with ν_{total} as in equation (23). On the other hand, that of the inflow to $C_{i,j,k}$ from $C_{i',j',k'}$, $P_{\text{coll}}(C_{i,j,k} \leftarrow C_{i',j',k'})$ in equation (21), is separated into $P_{\text{mom}}(C_{i,j,k} \leftarrow C_{i',j',k'})$, $P_{\text{exc}}(C_{i,j,k} \leftarrow C_{i',j',k'})$ and $P_{\text{ion}}(C_{i,j,k} \leftarrow C_{i',j',k'})$. Here, $P_{\text{coll}}(C_{i,j,k} \leftarrow C_{i',j',k'}) = 0$ when there is no direct electron transfer from $C_{i',j',k'}$ to $C_{i,j,k}$ via the collisional processes. It is assumed for $P_{\text{exc}}(C_{i,j,k} \leftarrow C_{i',j',k'})$ and $P_{\text{ion}}(C_{i,j,k} \leftarrow C_{i',j',k'})$ that $C_{i',j',k'}$ is a high-v cell and $C_{i,j,k}$ is a low-v one corresponding to the electron energy loss by the process. P_{att} is always zero because the electrons undergoing attachment are to disappear from velocity space and they have no destination cells.

Under the assumption of isotropic scattering, each of $C_{i,j,k}$ with a common i receives

a part of the scattered electrons in proportion to the solid angle $\Omega_{j,k}$ of $C_{i,j,k}$ subtended at O. In the present cell configuration,

$$\Omega_{j,k}=\int_{\theta_{j-1}}^{\theta_j}\int_{\phi_{k-1}}^{\phi_k}\sin\theta\ \mathrm{d}\theta\mathrm{d}\phi=(\cos\theta_{j-1}-\cos\theta_j)\Delta\phi. \tag{25}$$

$C_{i,j,k}$ and $C_{i',j',k'}$ for elastic momentum transfer collision are in the relation of $i=i'$ under an assumption that the elastic energy loss is negligible. $P_{\mathrm{mom}}(C_{i,j,k}\leftarrow C_{i',j',k'})$ is quantified with $\nu_{\mathrm{mom}}(v_{i'}^{\mathrm{R}})=Nq_{\mathrm{mom}}(v_{i'}^{\mathrm{R}})v_{i'}^{\mathrm{R}}$ as

$$P_{\mathrm{mom}}(C_{i,j,k}\leftarrow C_{i',j',k'})=\begin{cases}\dfrac{\Omega_{j,k}}{2\pi}\nu_{\mathrm{mom}}(v_{i'}^{\mathrm{R}}) & \text{for } i'=i\\ 0 & \text{for } i'\neq i\end{cases}. \tag{26}$$

Here, the denominator is not 4π but 2π, which represents that the scattered electrons are re-distributed only to the cells in the hemisphere of $v_y\geq 0$; the cells of $v_y\leq 0$ were omitted under the reflectional symmetry of the EVDF. The non-zero $P_{\mathrm{mom}}(C_{i,j,k}\leftarrow C_{i',j',k'})$ values satisfy

$$\sum_{j=1}^{j_{\max}/2}\sum_{k=1}^{k_{\max}}P_{\mathrm{mom}}(C_{i,j,k}\leftarrow C_{i',j',k'})=\nu_{\mathrm{mom}}(v_{i'}^{\mathrm{R}})\quad\text{for } i'=i. \tag{27}$$

For excitation, $C_{i,j,k}$ and $C_{i',j',k'}$ are related as $i'=i+l_{\mathrm{exc}}$, where $l_{\mathrm{exc}}=\lfloor\varepsilon_{\mathrm{exc}}/\Delta\varepsilon\rfloor$ is an integer representing the loss energy $\varepsilon_{\mathrm{exc}}$ of excitation discretized by $\Delta\varepsilon$. With $\nu_{\mathrm{exc}}(v_{i'}^{\mathrm{R}})=Nq_{\mathrm{exc}}(v_{i'}^{\mathrm{R}})v_{i'}^{\mathrm{R}}$,

$$P_{\mathrm{exc}}(C_{i,j,k}\leftarrow C_{i',j',k'})=\begin{cases}\dfrac{\Omega_{j,k}}{2\pi}\nu_{\mathrm{exc}}(v_{i'}^{\mathrm{R}}) & \text{for } i'=i+l_{\mathrm{exc}}\\ 0 & \text{for } i'\neq i+l_{\mathrm{exc}}\end{cases}, \tag{28}$$

$$\sum_{j=1}^{j_{\max}/2}\sum_{k=1}^{k_{\max}}P_{\mathrm{exc}}(C_{i,j,k}\leftarrow C_{i',j',k'})=\nu_{\mathrm{exc}}(v_{i'}^{\mathrm{R}})\quad\text{for } i'=i+l_{\mathrm{exc}}. \tag{29}$$

In case of ionization induced by a primary electron with energy $\varepsilon_{\mathrm{p}}'$, the residual energy $\varepsilon_{\mathrm{p}}'-\varepsilon_{\mathrm{ion}}$ after the subtraction of the ionization energy $\varepsilon_{\mathrm{ion}}$ is divided into two portions ε_{p} and ε_{s} for the primary and secondary electrons ($\varepsilon_{\mathrm{p}}'-\varepsilon_{\mathrm{ion}}=\varepsilon_{\mathrm{p}}+\varepsilon_{\mathrm{s}}$), and the number of electrons undergoing ionization is doubled to reflect the electron multiplication. In the present PM, the ratio $\varepsilon_{\mathrm{p}}:\varepsilon_{\mathrm{s}}$ was assumed to be equi-probable in a range between $0:1$ and $1:0$. $C_{i,j,k}$ and $C_{i',j',k'}$ are in the relation of $i'\geq i+l_{\mathrm{ion}}$, where $l_{\mathrm{ion}}=\lfloor\varepsilon_{\mathrm{ion}}/\Delta\varepsilon\rfloor$. $P_{\mathrm{ion}}(C_{i,j,k}\leftarrow C_{i',j',k'})$ is given with $\nu_{\mathrm{ion}}(v_{i'}^{\mathrm{R}})=Nq_{\mathrm{ion}}(v_{i'}^{\mathrm{R}})v_{i'}^{\mathrm{R}}$ as

$$P_{\mathrm{ion}}(C_{i,j,k}\leftarrow C_{i',j',k'})=\begin{cases}\dfrac{\Omega_{j,k}}{2\pi}\dfrac{4}{2(i'-l_{\mathrm{ion}})-1}\nu_{\mathrm{ion}}(v_{i'}^{\mathrm{R}}) & \text{for } i'>i+l_{\mathrm{ion}}\\ \dfrac{\Omega_{j,k}}{2\pi}\dfrac{2}{2(i'-l_{\mathrm{ion}})-1}\nu_{\mathrm{ion}}(v_{i'}^{\mathrm{R}}) & \text{for } i'=i+l_{\mathrm{ion}}\\ 0 & \text{for } i'<i+l_{\mathrm{ion}}\end{cases}. \tag{30}$$

The factors $2/[2(i'-l_{\rm ion})-1]$ and $4/[2(i'-l_{\rm ion})-1]$ approximate that the primary and secondary electrons originating in the ionization in $C_{i',j',k'}$ are re-distributed to the cells $C_{i,j,k}$ of $1\le i\le i'-l_{\rm ion}$, which correspond to an energy range $0\le\varepsilon\le\varepsilon'_{\rm p}-\varepsilon_{\rm ion}$, but the upper limit of this range varies between $\varepsilon_{i'-1}-\varepsilon_{\rm ion}$ for the ionization at $\varepsilon'_{\rm p}=\varepsilon_{i'-1}$ (i.e. the lower end of the energy range of $C_{i',j',k'}$) and $\varepsilon_{i'}-\varepsilon_{\rm ion}$ for the ionization at $\varepsilon'_{\rm p}=\varepsilon_{i'}$ (i.e. the upper end) [29]. For ionization in a cell $C_{i',j',k'}$,

$$\sum_{i=1}^{i'-l_{\rm ion}}\sum_{j=1}^{j_{\max}/2}\sum_{k=1}^{k_{\max}}P_{\rm ion}(C_{i,j,k}\leftarrow C_{i',j',k'})=2\nu_{\rm ion}(v_{i'}^{\rm R}). \tag{31}$$

3.6. Acceleration propagator

The change of electron velocity due to acceleration is continuous, thus the resulting intercellular electron transfer occurs between neighboring cells. The electron outflow from $C_{i,j,k}$ becomes the inflows to the neighboring destination cells $C_{i',j',k'}$ located in the downstream of $C_{i,j,k}$. $P_{\rm acc}(C_{i',j',k'}\leftarrow C_{i,j,k})$ is obtained from $\mathbf{a}$ on the boundary between $C_{i,j,k}$ and $C_{i',j',k'}$. Assuming uniform electron distribution within a cell, the electron outflow from $C_{i,j,k}$ is written as

$$\left(\frac{\partial}{\partial t}\right)_{\rm acc}^{\rm out}n_{i,j,k}=\left(K_{i-1,j,k}^{-v}+K_{i,j,k}^{+v}+K_{i,j-1,k}^{-\theta}+K_{i,j,k}^{+\theta}+K_{i,j,k-1}^{-\phi}+K_{i,j,k}^{+\phi}\right)\frac{n_{i,j,k}}{V_{i,j,k}} \tag{32}$$

$$K_{i,j,k}^{\pm *}=\int_{B_{i,j,k}^{*}}\max(\mathbf{a}\cdot(\pm\mathbf{n}^{*}),0)\,{\rm d}s_{i,j,k}^{*}, \tag{33}$$

where the asterisks represent v, θ or ϕ; $K_{i,j,k}^{\pm *}$ (≥ 0) are the rate coefficients of electron flows toward the $\pm v$, $\pm\theta$ and $\pm\phi$ directions through corresponding boundaries $B_{i,j,k}^{*}$; $\mathbf{n}^{*}$ are the unit normal vectors on $B_{i,j,k}^{*}$ toward the $+v$, $+\theta$ and $+\phi$ directions; and ${\rm d}s_{i,j,k}^{*}$ (≥ 0) are the areal elements of $B_{i,j,k}^{*}$. With the maximum function, that gives the greatest value among its arguments, only the positive values of $\mathbf{a}\cdot(\pm\mathbf{n}^{*})\,{\rm d}s_{i,j,k}^{*}$ are integrated to calculate the outflows separately from the inflow to $C_{i,j,k}$ from the neighbor cells. Therefore, some of $K_{i,j,k}^{\pm *}$ may be zero depending on the angle between $\mathbf{a}$ and $\mathbf{n}^{*}$. The acceleration propagators for the electron outflows from $C_{i,j,k}$ to its six neighbors are

$$P_{\rm acc}(C_{i-1,j,k}\leftarrow C_{i,j,k})=K_{i-1,j,k}^{-v}/V_{i,j,k}, \tag{34}$$

$$P_{\rm acc}(C_{i+1,j,k}\leftarrow C_{i,j,k})=K_{i,j,k}^{+v}/V_{i,j,k}, \tag{35}$$

$$P_{\rm acc}(C_{i,j-1,k}\leftarrow C_{i,j,k})=K_{i,j-1,k}^{-\theta}/V_{i,j,k}, \tag{36}$$

$$P_{\rm acc}(C_{i,j+1,k}\leftarrow C_{i,j,k})=K_{i,j,k}^{+\theta}/V_{i,j,k}, \tag{37}$$

$$P_{\rm acc}(C_{i,j,k-1} \leftarrow C_{i,j,k}) = K^{-\phi}_{i,j,k-1}/V_{i,j,k}. \tag{38}$$

$$P_{\rm acc}(C_{i,j,k+1} \leftarrow C_{i,j,k}) = K^{+\phi}_{i,j,k}/V_{i,j,k}, \tag{39}$$

In the present cell configuration under $\mathbf{E} \perp \mathbf{B}$, some of the borders at which $\mathrm{sgn}(\mathbf{a} \cdot \mathbf{n}^*)$ changes can be aligned at cell boundaries by letting $k_{\max}$ be an even integer, that simplifies the integral for $K^{\pm *}_{i,j,k}$. Their analytical derivations are presented in Appendix.

The calculated values of $P_{\rm acc}$ are stored to not six but four 3D arrays with the same size as for $n_{i,j,k}$. One is for $K^{\pm v}_{i,j,k}$. Because $K^{+v}_{i,j,k}$ or $K^{-v}_{i,j,k}$ is necessarily zero for each set of $\{i, j, k\}$ and whether $K^{+v}_{i,j,k} = 0$ or $K^{-v}_{i,j,k} = 0$ can be known from k, the storages for non-zero $K^{\pm v}_{i,j,k}$ can share a 3D array. $K^{\pm\theta}_{i,j,k}$ can be stored in a 3D array in the same way as $K^{\pm v}_{i,j,k}$. The directions of electron flows through the concentric boundaries $B^{v}_{i,j,k}$ and $B^{\theta}_{i,j,k}$ are unique on each of them. On the other hand, $K^{+\phi}_{i,j,k}$ and $K^{-\phi}_{i,j,k}$ may have non-zero values at the same time, i.e. the electron transfer through $B^{\phi}_{i,j,k}$ may be mutual between two neighboring cells $C_{i,j,k}$ and $C_{i,j,k+1}$. Thus, two different 3D arrays are needed to store $K^{\pm\phi}_{i,j,k}$. The condition of the mutual electron transfer is detailed in Appendix A.3.

3.7. Relaxation scheme

The equilibrium solution of the EVDF is obtained by iterative renewal of $n_{i,j,k}$ using equation (24) [29] in the manner of Gauss–Seidel method. The renewal was applied to the cells from the upstream to the downstream in velocity space so that the renewed values of $n_{i,j,k}$, which were expected to be closer to the equilibrium solution than their previous values, were used immediately for succeeding renewal of $n_{i,j,k}$ of other cells. The upstream and downstream were determined by the direction of $\mathbf{a}$. The relaxation was terminated when the relative changes of the electron transport parameters described in the next section became less than 10^{-7}.

Note that $\mathbf{a}$ in velocity space is rotational (see figure 1). On $B^{v}_{i,j,k}$ and $B^{\theta}_{i,j,k}$, $\mathbf{a}$ is toward the $+v$ and $+\theta$ directions in the region of $v_z \geq 0$, respectively. In the region of $v_z \leq 0$, their directions are opposite. These aspects are depicted in figure A1 in Appendix. On the other hand, $\mathbf{a}$ is toward the $-\phi$ direction on a majority of $B^{\phi}_{i,j,k}$, but there are opposite cases in the region of $v_x \geq 0$. This reverse directionality appears in a cylinder of infinite length having an axis $(v_x, v_z) = (\frac{1}{2}(E/B), 0)$ and a diameter E/B (see figures A2 and A4 in Appendix). Let us name this region 'reverse region' and its

outside region 'regular region' for later discussions.

On the basis of this directionality of $\mathbf{a}$, the sequence of the renewal of $n_{i,j,k}$ in triple nesting loops with indices i, j and k was arranged as follows.

For ϕ, the renewal was from $k = k_{\max}$ ($\phi = 2\pi$) to $k = 1$ ($\phi = 0$) by decrement of k. A modification for the renewal sequence on k in the region of $v_x \geq 0$ is attempted later in section 5.1.

For θ at a k, the renewal was from $j = \frac{1}{2}j_{\max}$ ($\theta = \frac{1}{2}\pi$) to $j = 1$ ($\theta = 0$) by decrement of j in the region of $v_z \leq 0$, and from $j = 1$ to $j = \frac{1}{2}j_{\max}$ by increment of j in the region of $v_z \geq 0$.

For v at a k and a j, the renewal was from $i = i_{\max}$ ($v = v_{\max}$) to $i = 1$ ($v = 0$) by decrement of i in the region of $v_z \leq 0$, and from $i = 1$ to $i = i_{\max}$ by increment of i in the region of $v_z \geq 0$.

4. Benchmark

Two gases were chosen for benchmark of the present PM calculation. One is a ramp model gas [46] having $q_{\mathrm{mom}} = 6.0 \times 10^{-16}\,\mathrm{cm}^2$ and $q_{\mathrm{exc}}(\varepsilon) = 10.0 \times 10^{-16} \times \max((\varepsilon - \varepsilon_{\mathrm{exc}})/\varepsilon_{1\mathrm{eV}}, 0)\,\mathrm{cm}^2$ with $\varepsilon_{\mathrm{exc}} = 0.2\,\mathrm{eV}$. The other is SF_6, which is a real gas having all of q_{mom}, q_{exc}, q_{ion} and q_{att} [47, 48]. The former and latter are examples of electron conservative and non-conservative cases, respectively.

The mean electron energy $\bar{\varepsilon}$ and components $W_{\mathbf{E}}$ and $W_{\mathbf{E}\times\mathbf{B}}$ of the average electron velocity vector $\mathbf{W} = (W_{\mathbf{E}\times\mathbf{B}}, W_{\mathbf{B}}, W_{\mathbf{E}}) = (\langle v_x\rangle, \langle v_y\rangle, \langle v_z\rangle)$ were derived from the EVDF as

$$\begin{aligned}
\bar{\varepsilon} = \frac{1}{2}m\langle v^2\rangle &= \frac{1}{N_{\mathrm{e}}}\int_{v_x=-\infty}^{\infty}\int_{v_y=-\infty}^{\infty}\int_{v_z=-\infty}^{\infty}\frac{1}{2}mv^2 f(v_x, v_y, v_z)\,\mathrm{d}v_x\mathrm{d}v_y\mathrm{d}v_z \\
&= \frac{1}{N_{\mathrm{e}}}\sum_{i=1}^{i_{\max}}\sum_{j=1}^{j_{\max}/2}\sum_{k=1}^{k_{\max}}\varepsilon_i^{\mathrm{R}}\, n_{i,j,k}, \qquad (40) \\
W_{\mathbf{E}\times\mathbf{B}} = \langle v_x\rangle &= \frac{1}{N_{\mathrm{e}}}\int_{v_x=-\infty}^{\infty}\int_{v_y=-\infty}^{\infty}\int_{v_z=-\infty}^{\infty} v_x f(v_x, v_y, v_z)\,\mathrm{d}v_x\mathrm{d}v_y\mathrm{d}v_z \\
&= \frac{1}{N_{\mathrm{e}}}\sum_{i=1}^{i_{\max}}\sum_{j=1}^{j_{\max}/2}\sum_{k=1}^{k_{\max}} v_i^{\mathrm{R}}\sin\theta_j^{\mathrm{R}}\cos\phi_k^{\mathrm{R}}\, n_{i,j,k}, \qquad (41) \\
W_{\mathbf{B}} = \langle v_y\rangle &= \frac{1}{N_{\mathrm{e}}}\int_{v_x=-\infty}^{\infty}\int_{v_y=-\infty}^{\infty}\int_{v_z=-\infty}^{\infty} v_y f(v_x, v_y, v_z)\,\mathrm{d}v_x\mathrm{d}v_y\mathrm{d}v_z = 0, \qquad (42) \\
W_{\mathbf{E}} = \langle v_z\rangle &= \frac{1}{N_{\mathrm{e}}}\int_{v_x=-\infty}^{\infty}\int_{v_y=-\infty}^{\infty}\int_{v_z=-\infty}^{\infty} v_z f(v_x, v_y, v_z)\,\mathrm{d}v_x\mathrm{d}v_y\mathrm{d}v_z
\end{aligned}$$

$$= \frac{1}{N_\mathrm{e}} \sum_{i=1}^{i_\mathrm{max}} \sum_{j=1}^{j_\mathrm{max}/2} \sum_{k=1}^{k_\mathrm{max}} v_i^\mathrm{R} \sin\theta_j^\mathrm{R} \sin\phi_k^\mathrm{R}\, n_{i,j,k}. \tag{43}$$

Here, $\theta_j^\mathrm{R} = (j-\frac{1}{2})\Delta\theta$ and $\phi_k^\mathrm{R} = (k-\frac{1}{2})\Delta\phi$ are the representative θ and ϕ values of $C_{i,j,k}$, respectively. $W_\mathbf{B} = 0$ when $\mathbf{E}\perp\mathbf{B}$ for the reflectional symmetry of the EVDF.

These parameters in the ramp model gas under $\mathbf{E}\times\mathbf{B}$ fields are available from the literature; those obtained by a BE analysis [49] and a MC simulation [50]. Note that $\mathbf{W}$ has been defined as the average velocity here but is identical to the centroid drift velocity in Ref. [50] under the present electron-conservative condition. The benchmark for the ramp model gas was performed at the reduced electric and magnetic fields, E/N and B/N, respectively, reported in Ref. [50]; 200 Hx at 1 Td; 1, 10, 50, 200 and 500 Hx at 12 Td; and 200 Hx at 24 Td. Here, 1 Td (townsend) = 10^{-21} Vm^2, and 1 Hx (huxlay) = 10^{-27} Tm^3. The size of the 3D arrays used in the PM, $i_\mathrm{max}\times\frac{1}{2}j_\mathrm{max}\times k_\mathrm{max}$, was chosen to be $12000\times45\times2160$. The initial EVDF was a Maxwellian with $\bar{\varepsilon} = 0.1$ eV. ε_max was set to be 1.2–3.0 eV. A part of the preliminary calculations was reported also in Ref. [32].

For SF_6, the parameters were calculated at combinations of E/N = 100, 200, 500, 1000 and 2000 Td and B/N = 100, 200, 500, 1000 and 2000 Hx (25 conditions in total) by the PM and a MC simulation. Some of the conditions were examined in previous work [30, 31, 33], but the condition has been extended to higher E/N and B/N values for the present benchmark. The initial EVDF was a Maxwellian with $\bar{\varepsilon} = 1.0$ eV, $\varepsilon_\mathrm{max} = 100.0$ eV and $i_\mathrm{max}\times\frac{1}{2}j_\mathrm{max}\times k_\mathrm{max} = 10000\times45\times720$. In the MC simulations, the time step Δt was set at 0.1 ps at $N = 10^{22}$ m^{-3}. Trace times of 100–200 ns were necessary in most cases to obtain the parameters in equilibrium. The number of electrons traced was more than 10^6. At E/N = 100 Td and B/N = 2000 Hx, the electron population decreased severely and the relaxation time was taken to be 500 ns for slow relaxation. Because it was difficult to acquire a sufficient number of samples in equilibrium, a technique of the periodic sample multiplication [51] was adopted in this condition.

Primary properties (CPU, clock frequency, main memory and operating system) of the workstations used for the benchmark were as follows. Intel Xeon E5-2667 (6-core), 2.9 GHz, 32 GB, and Linux CentOS 6.4 for the ramp model gas; and Intel Xeon E5-1650 v4 (6-core), 3.6 GHz, 128 GB, and Linux CentOS 7.3 for SF_6. Programming language was C++. The latter machine was able to perform at most four PM calculations in

parallel. The limit was from the required memory capacity.

4.1. Results of ramp model gas

Table 1 shows a comparison of $\bar{\varepsilon}$, $W_{\mathbf{E}\times\mathbf{B}}$ and $W_{\mathbf{E}}$ in the ramp model gas. The ratios of the PM results to those of the BE analysis are shown together. The parameters agreed well with each other with discrepancies less than 1% in most cases. The relaxation cycles required for the convergence of these results were 66–200, when the accelerated relaxation scheme tested in section 5.1 was used. The CPU times were 2.2–6.9 h, roughly being proportional to the relaxation cycles (about 2.0 min per relaxation cycle).

The discrepancies more than 1% were seen in the cases of 1 Hx at 12 Td, 500 Hx at 12 Td and 200 Hx at 1 Td. The discrepancy in the former one (the CPU time was 2.3 h for 68 cycles) seems to be simply due to small absolute value of the parameter. On the other hand, the latter two (27.6 h for 836 relaxation cycles and 228.1 h for 3446 relaxation cycles, respectively) are considered to be severe conditions as indicated by the long CPU times. There was a tendency that the discrepancy became large and the relaxation became long when the Hall deflection angle $\theta_{\mathrm{H}} = \tan^{-1}(W_{\mathbf{E}\times\mathbf{B}}/W_{\mathbf{E}})$ was large under high B/N, although the discrepancies were at most a few percent. Here, θ_{H} represents the significance of $\mathbf{B}$ relative to that of $\mathbf{E}$ in determining the equilibrium EVDF. In the ramp model gas, the inelastic collisions, by which the energy relaxation of the electrons proceeds mainly, are less frequent than the electron cyclotron motion quantified by ω $(= eB/m)$ when $\bar{\varepsilon}$ is low under strong $\mathbf{B}$. From the viewpoint of the numerical relaxation, one might expect that a high ω enhances the intercellular electron transfer by accelerating the rotational electron flow in velocity space and this enhancement might promote the relaxation of the EVDF. However, the high ω did not contribute to the energy relaxation. This is because the electron flow across $B^{v}_{i,j,k}$, that induces the change of ε, does not increase with ω; the rotation center represented as $(v_x, v_z) = (E/B, 0)$ approaches the v_y-axis as B increases, that reduces the change of ε accompanying the rotational electron flow. This can be understood from equations (A.9), (A.12), (A.23) and (A.26), in which $K^{\pm v}_{i,j,k}$ are independent of B (canceled in their factor $\omega(E/B)$) while $K^{\pm\phi}_{i,j,k}$ have terms proportional to ω.

Table 1. Comparison of mean electron energy $\bar{\varepsilon}$, components $W_{\mathbf{E}}$ and $W_{\mathbf{E}\times\mathbf{B}}$ of average electron velocity vector $\mathbf{W}$, and the Hall deflection angle θ_{H} in ramp model gas [46]. BE, Boltzmann equation analysis [49]; MC, Monte Carlo simulation [50]; and PM, propagator method (present).

E/N (Td)	B/N (Hx)	Method Ratio	$\bar{\varepsilon}$ (eV)	$W_{\mathbf{E}}$ ($10^4\,\mathrm{m\,s^{-1}}$)	$W_{\mathbf{E}\times\mathbf{B}}$ ($10^4\,\mathrm{m\,s^{-1}}$)	θ_{H} (deg)
1	200	BE	0.06821	0.1446	0.4488	72.1
		MC	0.0658	0.1437	0.4498	72.3
		PM	0.07053	0.1483	0.4464	71.6
		PM/BE (%)	103.40	102.55	99.46	99.25
12	1	BE	0.2689	6.838	0.04151	0.348
		MC	0.2693	6.833	0.0417	0.350
		PM	0.26893	6.8262	0.04092	0.343
		PM/BE (%)	100.01	99.83	98.58	98.75
12	10	BE	0.2687	6.821	0.4146	3.48
		MC	0.2690	6.818	0.4149	3.48
		PM	0.26865	6.8090	0.41282	3.47
		PM/BE (%)	99.98	99.82	99.57	99.75
12	50	BE	0.2616	6.401	2.020	17.5
		MC	0.2616	6.400	2.0192	17.5
		PM	0.26157	6.3905	2.0123	17.5
		PM/BE (%)	99.99	99.84	99.62	99.80
12	200	BE	0.1816	2.573	4.208	58.9
		MC	0.1817	2.571	4.204	58.6
		PM	0.18202	2.5800	4.1938	58.4
		PM/BE (%)	100.23	100.27	99.66	99.13
12	500	BE	0.1123	0.4154	2.318	79.8
		MC	0.1124	0.4161	2.318	79.8
		PM	0.11370	0.42293	2.3146	79.6
		PM/BE (%)	101.24	101.81	99.85	99.76
24	200	BE	0.3192	5.516	5.688	45.9
		MC	0.31944	5.509	5.686	45.9
		PM	0.31957	5.5165	5.6632	45.8
		PM/BE (%)	100.12	100.01	99.56	99.72

4.2. Results of SF_6

The parameters in SF_6 are presented in table 2. Most of them agreed well between the PM and MC results with discrepancies less than 1%. Similarly to the results of the ramp model gas, discrepancies exceeding 1% were seen in case the absolute value of the parameter is small.

The CPU times required for the relaxation cycles N_{alt} in table 3 shown later, using the accelerated relaxation scheme in section 5.1, were about 0.8–27.7 h (0.78–0.88 min per relaxation cycle). The CPU times of the MC simulations, which depend on the number of traced electrons and the trace time steps, however, were about 1.9–118.4 h. The conditions at $E/N = 100$–200 Td and $B/N = 2000$ Hx at 500 Td were attachment-dominant. Decrease of electrons with time made the MC simulations time-consuming to have a sufficient number of electrons in equilibrium, but the PM obtained equilibrium EVDF solutions stably.

Table 2. Mean electron energy $\bar{\varepsilon}$ and components $W_{\mathbf{E}}$ and $W_{\mathbf{E}\times\mathbf{B}}$ of average electron velocity vector $\mathbf{W}$ in SF_6 [47, 48] at combinations of $E/N = 100$, 200, 500, 1000 and 2000 Td and $B/N = 100$, 200, 500, 1000 and 2000 Hx. MC, Monte Carlo simulation; and PM, propagator method.

E/N	$B/N = 100$ Hx			$B/N = 200$ Hx			$B/N = 500$ Hx			$B/N = 1000$ Hx			$B/N = 2000$ Hx		
Method	$\bar{\varepsilon}$	$W_{\mathbf{E}}$	$W_{\mathbf{E}\times\mathbf{B}}$	$\bar{\varepsilon}$	$W_{\mathbf{E}}$	$W_{\mathbf{E}\times\mathbf{B}}$	$\bar{\varepsilon}$	$W_{\mathbf{E}}$	$W_{\mathbf{E}\times\mathbf{B}}$	$\bar{\varepsilon}$	$W_{\mathbf{E}}$	$W_{\mathbf{E}\times\mathbf{B}}$	$\bar{\varepsilon}$	$W_{\mathbf{E}}$	$W_{\mathbf{E}\times\mathbf{B}}$
Ratio	(eV)	(10^4 m s^{-1})		(eV)	(10^4 m s^{-1})		(eV)	(10^4 m s^{-1})		(eV)	(10^4 m s^{-1})		(eV)	(10^4 m s^{-1})	
100 Td															
MC	5.413	6.392	0.442	5.399	6.289	0.852	5.316	5.783	1.983	5.113	4.447	3.046	4.951	2.340	3.129
PM	5.423	6.370	0.434	5.410	6.287	0.857	5.329	5.761	1.963	5.140	4.441	3.013	4.985	2.356	3.104
PM/MC (%)	100.20	99.67	98.28	100.21	99.96	100.59	100.23	99.63	99.98	100.53	99.87	98.91	100.67	100.72	99.19
200 Td															
MC	6.598	11.432	0.682	6.583	11.330	1.380	6.473	10.596	3.230	6.139	8.559	5.281	5.430	4.738	6.053
PM	6.602	11.425	0.692	6.586	11.311	1.371	6.476	10.572	3.216	6.148	8.550	5.263	5.456	4.749	6.010
PM/MC (%)	100.07	99.94	101.42	100.04	99.83	99.38	100.04	99.77	99.56	100.15	99.89	99.66	100.49	100.23	99.29
500 Td															
MC	9.320	23.927	1.205	9.304	23.770	2.382	9.181	22.713	5.762	8.776	19.481	10.077	7.722	12.098	13.023
PM	9.321	23.897	1.198	9.304	23.741	2.383	9.182	22.678	5.737	8.778	19.453	10.026	7.702	12.110	12.969
PM/MC (%)	100.01	99.88	99.44	99.99	99.88	100.06	100.01	99.84	99.56	100.02	99.86	99.49	99.75	100.09	99.58
1000 Td															
MC	12.596	40.450	1.675	12.579	40.274	3.346	12.469	39.077	8.208	12.061	35.061	15.155	10.802	24.069	22.015
PM	12.592	40.381	1.673	12.577	40.208	3.337	12.467	39.009	8.170	12.060	35.022	15.080	10.698	24.053	21.944
PM/MC (%)	99.97	99.83	99.90	99.98	99.84	99.74	99.98	99.83	99.54	99.99	99.89	99.51	99.04	99.93	99.68
2000 Td															
MC	17.883	64.299	2.045	17.867	64.176	4.140	17.763	63.111	10.203	17.397	59.294	19.718	15.887	46.083	33.220
PM	17.864	64.186	2.056	17.849	64.034	4.106	17.749	62.966	10.172	17.384	59.192	19.632	15.887	46.026	33.048
PM/MC (%)	99.89	99.82	100.52	99.90	99.78	99.18	99.92	99.77	99.70	99.93	99.83	99.56	100.00	99.88	99.48

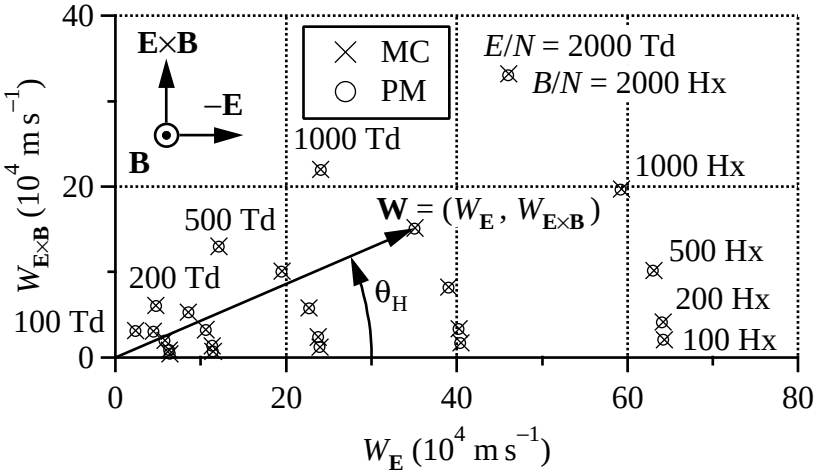

Figure 4. Components $W_{\mathbf{E}}$ and $W_{\mathbf{E}\times\mathbf{B}}$ of the average electron velocity vector $\mathbf{W}$. $|\mathbf{W}| = (W_{\mathbf{E}}^2 + W_{\mathbf{E}\times\mathbf{B}}^2)^{1/2}$ and θ_{H} increase with E/N and B/N, respectively.

An aspect of the Hall deflection is depicted in figure 4 using $W_{\mathbf{E}}$ and $W_{\mathbf{E}\times\mathbf{B}}$ in table 2. The increase of $|\mathbf{W}|$ with E/N and that of θ_{H} with B/N are observed clearly.

Figure 5 shows the EVDF at 1000 Td and 1000 Hx. The EVDF has been projected to the $v_x v_z$-plane as

$$f(v_x, v_z) = \int_{v_y=-\infty}^{\infty} f(v_x, v_y, v_z)\, \mathrm{d}v_y, \tag{44}$$

and has been normalized to satisfy

$$\int_{v_x=-\infty}^{\infty} \int_{v_z=-\infty}^{\infty} f(v_x, v_z)\, \mathrm{d}v_x \mathrm{d}v_z = 1. \tag{45}$$

The scales for v_x and v_z are expressed in unit of $v_{1\mathrm{eV}}$ as $v_x/v_{1\mathrm{eV}}$ and $v_z/v_{1\mathrm{eV}}$ so that the conversion from speed to energy is easy; the value of $(v/v_{1\mathrm{eV}})^2$ gives the value of the energy in eV. At $E/N = 1000\,\mathrm{Td}$ and $B/N = 1000\,\mathrm{Hx}$, the rotation center of $\mathbf{a}$ is at $(v_x/v_{1\mathrm{eV}}, v_z/v_{1\mathrm{eV}}) = (1.686, 0)$, where the $\mathbf{E} \times \mathbf{B}$ drift velocity is $E/B = 10^6\,\mathrm{ms}^{-1} = 1.686 \times v_{1\mathrm{eV}}$.

The PM successfully reproduced the EVDF obtained by the MC. The fluctuation-free PM solution enables us to observe the shape of EVDF in detail. For example, the EVDF peak shifted from the origin to $(v_x/v_{1\mathrm{eV}}, v_z/v_{1\mathrm{eV}}) = (0.5, 0.8)$. The angle of the peak direction $\tan^{-1}(0.5/0.8) = 32.0°$ was greater than $\theta_{\mathrm{H}} = 23.2°$ of $\mathbf{W}$. The distribution width in figure 5(b) along the $\mathbf{E}$ direction is about 3% narrower than that in figure 5(c) along the $\mathbf{E} \times \mathbf{B}$ direction. The EVDF is close to a Gaussian around the peak, but it has a slight asymmetry.

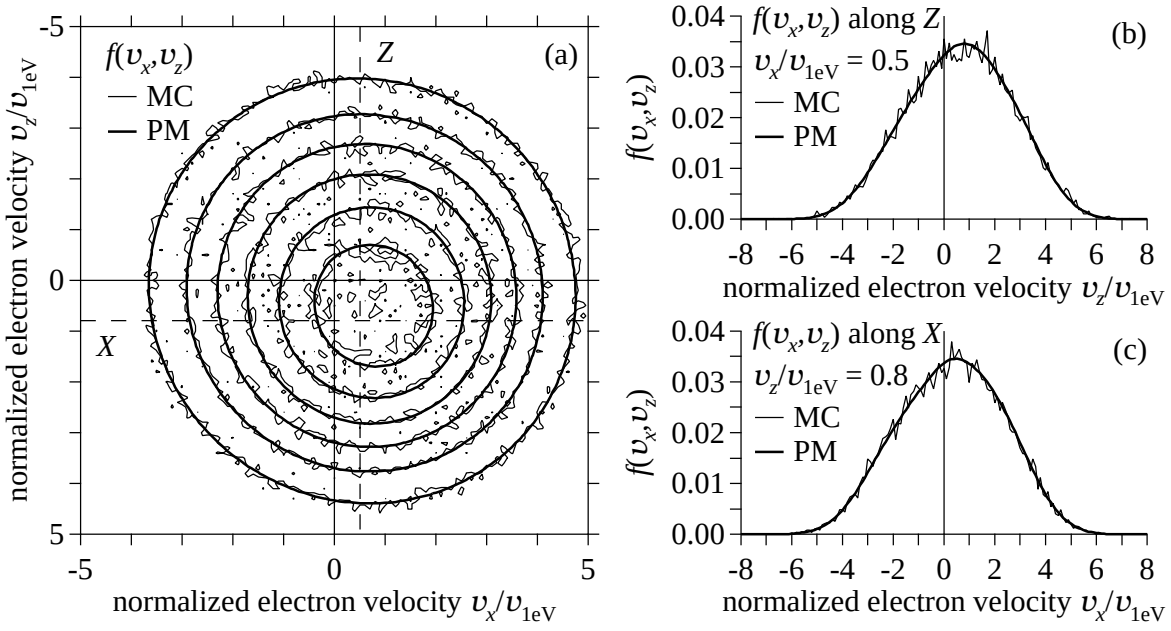

Figure 5. The EVDF in SF_6 at $E/N = 1000\,\mathrm{Td}$ and $B/N = 1000\,\mathrm{Hx}$. (a) contours of $f(v_x, v_z)$ from 0.005 to 0.030 in steps of 0.005, (b) $f(v_x, v_z)$ along cross section Z at $v_x/v_{1\mathrm{eV}} = 0.5$, and (c) $f(v_x, v_z)$ along cross section X at $v_z/v_{1\mathrm{eV}} = 0.8$. v_x and v_z are the velocity components in the directions of $\mathbf{E} \times \mathbf{B}$ and $-\mathbf{E}$, respectively. $f(v_x, v_z)$ has its peak at the intersection between X and Z.

5. Discussion

5.1. Further acceleration of numerical relaxation

The renewal of $n_{i,j,k}$ was made by decrement of k for ϕ. However, locally in the reverse region, this renewal direction was against the upstream-to-downstream policy and it is considered that this retarded the convergence of the EVDF. Thus, as a simple modification, the renewal direction was rearranged to be back-and-forth. In the modified relaxation scheme, increment and decrement of k were alternated every other relaxation cycles in the region of $v_x \geq 0$, where the reverse region lies. It is expected that the increment of k would accelerate the relaxation in the reverse region, while it would retard the relaxation in the regular region.

Table 3 shows the relaxation cycles to achieve the seven-digit convergence before and after the above modification. N_{fix} represents the cycles in the decrement-only cases, and N_{alt} is of alternated decrement and increment. The convergence was judged after

Table 3. Comparison of relaxation cycles $(N_{\rm fix}, N_{\rm alt})$ required for seven-digit convergence in calculation of the EVDF in SF_6 by the PM at various E/N (Td) and B/N (Hx). $N_{\rm fix}$, renewal of $n_{i,j,k}$ by decrement of k only; and $N_{\rm alt}$, by alternated decrement and increment of k.

E/N	B/N				
	100 Hx	200 Hx	500 Hx	1000 Hx	2000 Hx
100 Td	(1544, 566)	(1304, 606)	(1146, 744)	(1146, 1068)	(1434, 1980)
200 Td	(1826, 300)	(1550, 310)	(1308, 362)	(1246, 506)	(1314, 990)
500 Td	(1668, 138)	(1528, 136)	(1334, 152)	(1324, 194)	(1780, 376)
1000 Td	(1362, 78)	(1250, 76)	(1134, 80)	(942, 92)	(1238, 146)
2000 Td	(1220, 54)	(1038, 52)	(1162, 52)	(1114, 58)	(1010, 76)

every two cycles for $N_{\rm fix}$ and every pair of decrement and increment cycles for $N_{\rm alt}$. The result was $N_{\rm alt} < N_{\rm fix}$ in most cases as expected. The acceleration in the reverse region exceeded the retardation outside in total. The only exception was the case of 100 Td at 2000 Hx, in which the diameter E/B of the reverse region is the smallest.

Implementation of the upstream-to-downstream renewal of $n_{i,j,k}$ throughout the cells both in the reverse and regular regions might lead to faster relaxation. The criterion to judge whether $C_{i,j,k}$ belongs to the reverse region or not with the indices i, j and k is definite as described in Appendix. However, a sequence to realize the upstream-to-downstream renewal seems to be not simple in the off-axis rotational field of **a** because the seeking for the indices corresponding to the border between the regular and reverse regions requires a case analysis in the present cell configuration. The locally specific treatment for the reverse region would increase the load to manage the indices of the triple nesting loops and it might prevent efficient parallel processing. The optimization of the relaxation sequence is left as a technical issue in the practical coding together with investigation on efficient treatment of the mutual electron flows in the upstream-to-downstream renewal scheme.

5.2. Extension for real-space electron transport parameters

The parameters derived from the EVDF in the present work, $\bar{\varepsilon}$, $W_{\mathbf{E}\times\mathbf{B}}$ and $W_{\mathbf{E}}$, do not require information on the electron position in real space. On the other hand, the rate coefficients of some other electron reactions would be derived from the EVDF

using corresponding collision cross sections by assuming position-dependent factors such as the number densities of electrons and excited/ionic species, because the present PM is to obtain normalized EVDF. Furthermore, there are demands for real-space electron transport parameters such as the centroid drift velocity $\mathbf{W}_\mathrm{r} = (W_{\mathrm{r},x}, W_{\mathrm{r},y}, W_{\mathrm{r},z})$ and the diffusion coefficients $D_{\mathrm{r},x}$, $D_{\mathrm{r},y}$ and $D_{\mathrm{r},z}$ along specific directions x, y and z, respectively, for fluid model simulations and theoretical studies on the electron transport in magnetized plasmas. A theory to derive these real-space parameters from moment equations has already been established for electron swarms under dc $\mathbf{E}$ [18, 19, 20, 21, 52]. This theory was applied to electron swarms under $\mathbf{E} \times \mathbf{B}$ fields of $\mathbf{E} \perp \mathbf{B}$ [30]. $W_{\mathrm{r},x}$, $W_{\mathrm{r},y}$ and $W_{\mathrm{r},z}$ were derived from the first-order x, y and z moments, and $D_{\mathrm{r},x}$, $D_{\mathrm{r},y}$ and $D_{\mathrm{r},z}$ were obtained from the second-order ones. The accelerated relaxation scheme [29] and the propagators were applicable commonly to the higher-order moments.

The zeroth-, first- and second-order moment equations in a direction are in a hierarchy; i.e., a higher-order moment is dependent on those of lower orders. However, they can be calculated independently for each of the x, y and z directions. Thus, we need at least two more 3D arrays with the same size as for the zeroth-order moment $n_{i,j,k}$ to perform a PM calculation for a pair of $W_{\mathrm{r},x}$ and $D_{\mathrm{r},x}$, $W_{\mathrm{r},y}$ and $D_{\mathrm{r},y}$, or $W_{\mathrm{r},z}$ and $D_{\mathrm{r},z}$. Because the PM calculation can proceed sequentially for these pairs, the two 3D arrays for the first- and second-order moments with respect to a direction can be reused for the calculations of those of another direction, that saves the required memory capacity.

5.3. Extension for ac electric fields with dc and ac magnetic fields

A time-dependent acceleration propagator $P_\mathrm{acc}(t)$ is necessary for calculations of the EVDF under ac $\mathbf{E}$. The accelerated relaxation scheme [29] is no longer applicable here. The relaxation of the EVDF to a periodic steady state must proceed along physical time passage step by step for every Δt to be set by partitioning the ac phase 0–2π with a satisfactory time resolution. $P_\mathrm{acc}(t)$ is to be periodic, thus, it would be efficient in practical operation if all of the $P_\mathrm{acc}(t)$ values at the discretized ac phases could be stored in 3D arrays for repeated use. However, the memory capacity required for them would increase correspondingly to the number of the discretized phases. Nonetheless, most of the $P_\mathrm{acc}(t)$ properties are proportional to $|\mathbf{E}|$, that enables us to reduce the

necessity of additional 3D arrays by separating the time-dependent factor as a periodic weight.

First, when $E_z(t) = -E \sin \omega_{\rm ac} t$ and $\mathbf{B}$ is dc, $K^{\pm v}_{i,j,k}(t)$ and $K^{\pm \theta}_{i,j,k}(t)$ do not require additional 3D arrays. Their non-zero values are proportional to $|E_z(t)|$ as inferred from equations (A.9)–(A.12) and (A.16)–(A.19), and thus they can be represented in a form of $K^{\pm *}_{i,j,k,\max} |\sin \omega_{\rm ac} t|$ ($*$: v or θ). Their amplitudes $K^{\pm *}_{i,j,k,\max}$ are constant and can be stored in existing 3D arrays instead of $K^{\pm *}_{i,j,k}$ under dc $\mathbf{E}$. $K^{\pm v}_{i,j,k}(t)$ would vary in a manner of half-wave rectification complementarily, and $K^{\pm \theta}_{i,j,k}(t)$ would vary similarly. On the other hand, $K^{\pm \phi}_{i,j,k}(t)$ would need additional 3D arrays. $K^{\pm \phi}_{i,j,k}(t)$ of such $B^{\phi}_{i,j,k}$ that locate always outside of the reverse region can be represented by $\mathbf{E}$-independent (constant) and $\mathbf{E}$-dependent (sinusoidal) terms as seen in equations (A.25) and (A.26). They would need one additional 3D array to store the amplitude of the sinusoidal term in addition to the constant term. The other $K^{\pm \phi}_{i,j,k}(t)$ would need further 3D arrays because the reverse region, whose diameter is $(E/B)|\sin \omega_{\rm ac} t|$, expands and shrinks periodically, and $K^{\pm \phi}_{i,j,k}(t)$ of $B^{\phi}_{i,j,k}$ which may have an intersection with the boundary of the reverse region are calculated under a case analysis to choose applicable equations from equations (A.23)–(A.26), (A.49), (A.56), (A.61) and (A.65).

Next, when $\mathbf{E}$ and $\mathbf{B}$ are both ac and they alternate synchronously as $E_z(t) = -E \sin \omega_{\rm ac} t$ and $B_y(t) = B \sin \omega_{\rm ac} t$, $E_z(t)/B_y(t)$ is constant. In such a field condition, i.e. in electromagnetic wave, all non-zero $K^{\pm *}_{i,j,k}(t)$ would be represented in a form of $K^{\pm *}_{i,j,k,\max} |\sin \omega_{\rm ac} t|$ because all components of $\mathbf{a}$ in equation (A.2) varies in proportion to ω ($= eB_z(t)/m \propto \sin \omega_{\rm ac} t$) keeping the direction of $\mathbf{a}$ unchanged in the rotational field, i.e. the reverse region is unchanged throughout the ac phase. Thus, the PM calculation under synchronous ac $\mathbf{E}$ and ac $\mathbf{B}$ would not require additional 3D arrays.

Furthermore, when ac $\mathbf{E}$ and ac $\mathbf{B}$ have a phase difference, e.g. $E_z(t) = -E \sin \omega_{\rm ac} t$ and $B_y(t) = B \cos \omega_{\rm ac} t$, as assumed in Refs. [53, 54, 55], $P_{\rm acc}(t)$ would be prepared similarly to that under ac $\mathbf{E}$ and dc $\mathbf{B}$. The non-zero values of $K^{\pm v}_{i,j,k}(t)$ and $K^{\pm \theta}_{i,j,k}(t)$ are proportional to $|E_z(t)|$, and the calculation of $K^{\pm \phi}_{i,j,k}(t)$ requires a case analysis whether the boundary of the reverse region intersects $B^{\phi}_{i,j,k}$ or not. Here, all $B^{\phi}_{i,j,k}$ may be included in the reverse region because $(E/B) \tan \omega_{\rm ac} t$, whose absolute value represents the diameter of the reverse region, may diverge to $\pm\infty$.

5.4. Extension for $\mathbf{E} \times \mathbf{B}$ *fields crossed at arbitrary angles*

The condition $\mathbf{E} \perp \mathbf{B}$, in which $\mathbf{a}$ is parallel to the $v_x v_z$-plane, allowed us to quantify P_{acc} analytically. In contrast, when $\mathbf{E} \not\perp \mathbf{B}$ [55, 56, 57, 58], the directionality of $\mathbf{a}$ crossing the cell boundaries would vary in a complicated way for $B^{v}_{i,j,k}$ and $B^{\theta}_{i,j,k}$ because $\mathbf{a}$ becomes helical. It has never been investigated how far the derivation of P_{acc} could be carried out analytically in such a condition. It might become fully numerical integration of $\max(\mathbf{a} \cdot \mathbf{n}, 0)\, \mathrm{d}s$ for each boundary. In that case, a cell boundary would be divided into small areal elements with respect to the two variables consisting $\mathrm{d}s$, and judgement of $\mathrm{sgn}(\mathbf{a} \cdot \mathbf{n})$ is made on each element. This calculation is for 3D arrays, thus the total calculation may include up to quintuple loops. In addition, the cells for $v_y \leq 0$ cannot be omitted in the absence of the reflectional symmetry in the EVDF. This would be a heavy load even for the latest computers.

6. Conclusions

A technique of the PM to calculate the EVDF under $\mathbf{E} \perp \mathbf{B}$ was detailed. Under the $\mathbf{E} \times \mathbf{B}$ fields, the EVDF becomes non-axisymmetric because the electron acceleration vector $\mathbf{a}$ is of off-axis rotation in velocity space. Velocity space was divided into cells by partitioning the three polar coordinates v, θ and ϕ, and corresponding 3D arrays were prepared to store the number of electrons in each cell and the rate coefficients of the electron outflows from the cell across its boundaries. The rate coefficients were derived analytically from surface integrals of the inner product between $\mathbf{a}$ and the unit normal vector on the cell boundary.

Mean electron energy $\bar{\varepsilon}$ and components of the average electron velocity vector $W_{\mathbf{E}\times\mathbf{B}}$ and $W_{\mathbf{E}}$ in the ramp model gas and SF_6 were derived from the EVDF obtained by the PM. They agreed well with those obtained by a BE analysis and MC simulations. The discrepancies were mostly less than 1%, and were 1–3% under strong $\mathbf{B}$ or in case the calculated values were small. It is an advantage of the PM that smooth EVDF is obtained avoiding the statistical fluctuation inevitable in the MC simulations. The PM was stable even under conditions of $\bar{\nu}_{\mathrm{ion}} < 0$, where the MC simulations became difficult or much time-consuming because of the electron decrease before reaching the equilibrium.

An accelerated relaxation scheme based on the Gauss–Seidel method worked well. The renewal of the number of electrons in each cell was operated mainly from the upstream to the downstream in velocity space along the direction of **a**. The seven-digit convergence of the EVDF to its equilibrium solution was achieved in hundreds to thousands relaxation cycles. In the present cell configuration, there was a region in which the direction of **a** is locally reversed relative to a group of cell boundaries. This was because the rotation center of **a** is off-axis in velocity space. The upstream-to-downstream relaxation has not been implemented perfectly to all of the cells in the reverse region for the complexity in making a sequential operation order for the cells. However, an attempt showed that faster convergence is available simply by switching the renewal direction back and forth in the quadrants of velocity space including the reverse region.

A key achievement in composing the PM calculation code for the EVDF under crossed **E** and **B** was the derivation of the acceleration propagator. On the other hand, analysis of the precision depending on the cell configuration and resolution and improvement of the convergence speed are still left for further investigations. Extensions of the PM to calculations of the EVDF under ac **E** and dc/ac **B** and under **E** and **B** crossed at arbitrary angles were mentioned as possible succeeding work, however, such calculations would be much heavier than in the present work. Nonetheless, use of mainframe machines and/or further progress in computational resources would enable us to challenge them.

Acknowledgements

This work was supported by a KAKENHI grant JP16K05626 from the Japan Society for the Promotion of Science. This work was in part promoted in the activity of the AED1099 investigating R&D committee on techniques for gas-phase simulations of electric discharges and plasmas in the Institute of Electrical Engineers of Japan. The author wishes to thank Ms. Suzu Matsumoto and Mr. Yuta Kubo of Hokkaido University for their assistance in the benchmark calculations.

Appendix A. Electron flow through cell boundaries

In order to quantify the acceleration propagator $P_{\rm acc}(C_{i',j',k'} \leftarrow C_{i,j,k})$ in equations (34)–(39), which represents the electron flow from a source cell $C_{i,j,k}$ to a neighboring destination cell $C_{i',j',k'}$ through the cell boundary between $C_{i,j,k}$ and $C_{i',j',k'}$ under the action of the $\mathbf{E}\times\mathbf{B}$ fields, the rate coefficients $K^{\pm *}_{i,j,k}$ ($*$: v, θ or ϕ) of the electron flow are calculated in this section by the integral of $\mathbf{a}\cdot\mathbf{n}\,{\rm d}s$. Here, $\mathbf{a}$ is the electron acceleration by the $\mathbf{E}\times\mathbf{B}$ fields, $\mathbf{n}$ is the unit normal vector on the cell boundary, and ${\rm d}s$ (≥ 0) is the areal element of the boundary.

From equations (5)–(7), $\mathbf{a}$ is represented as

$$\begin{aligned}\mathbf{a} &= (\omega v_z, \omega\frac{E}{B}\cos\alpha, -\omega v_x + \omega\frac{E}{B}\sin\alpha)\\ &= (\omega v\sin\theta\sin\phi, \omega\frac{E}{B}\cos\alpha, -\omega v\sin\theta\cos\phi + \omega\frac{E}{B}\sin\alpha).\end{aligned} \tag{A.1}$$

Hereafter, we assume $\mathbf{E}\perp\mathbf{B}$, then

$$\mathbf{a} = (\omega v\sin\theta\sin\phi, 0, -\omega v\sin\theta\cos\phi + \omega\frac{E}{B}). \tag{A.2}$$

For the reflectional symmetry of the EVDF with respect to the v_xv_z-plane, $P_{\rm acc}(C_{i',j',k'} \leftarrow C_{i,j,k})$ is calculated only for the cells in the region of $v_y \geq 0$ ($C_{i,j,k}$ of $1 \leq j \leq \frac{1}{2}j_{\max}$).

Let K, $\mathbf{n}$ and ${\rm d}s$ have indices i, j and k and superscripts v, θ and ϕ when we distinguish them for individual boundaries $B^v_{i,j,k}$, $B^\theta_{i,j,k}$ and $B^\phi_{i,j,k}$ defined in equations (15)–(17). Here, the superscripts for K are signed to distinguish the direction of the electron flow. Equation (33) for K is rewritten as

$$K^{\pm v}_{i,j,k} = \int_{\theta=\theta_{j-1}}^{\theta_j}\int_{\phi=\phi_{k-1}}^{\phi_k} \max(\mathbf{a}\cdot(\pm\mathbf{n}^v_{i,j,k}), 0)\,{\rm d}s^v_{i,j,k}, \tag{A.3}$$

$$K^{\pm\theta}_{i,j,k} = \int_{v=v_{i-1}}^{v_i}\int_{\phi=\phi_{k-1}}^{\phi_k} \max(\mathbf{a}\cdot(\pm\mathbf{n}^\theta_{i,j,k}), 0)\,{\rm d}s^\theta_{i,j,k}, \tag{A.4}$$

$$K^{\pm\phi}_{i,j,k} = \int_{v=v_{i-1}}^{v_i}\int_{\theta=\theta_{j-1}}^{\theta_j} \max(\mathbf{a}\cdot(\pm\mathbf{n}^\phi_{i,j,k}), 0)\,{\rm d}s^\phi_{i,j,k}, \tag{A.5}$$

where $\mathbf{n}^v_{i,j,k}$, $\mathbf{n}^\theta_{i,j,k}$, and $\mathbf{n}^\phi_{i,j,k}$ are the unit normal vectors on $B^v_{i,j,k}$, $B^\theta_{i,j,k}$ and $B^\phi_{i,j,k}$ toward the $+v$, $+\theta$ and $+\phi$ directions, respectively. Analytical derivations of $K^{\pm v}_{i,j,k}$, $K^{\pm\theta}_{i,j,k}$ and $K^{\pm\phi}_{i,j,k}$ are presented in the following subsections.

The maximum functions in equations (33) and (A.3)–(A.5) are to integrate the positive and negative values of $\mathbf{a}\cdot\mathbf{n}$ separately. In the present cell configuration, we can arrange the cells so that ${\rm sgn}(\mathbf{a}\cdot\mathbf{n})$ is unchanged on all individual $B^v_{i,j,k}$ and $B^\theta_{i,j,k}$ as shown in Appendix A.1 and Appendix A.2. In such cases, we can omit the maximum

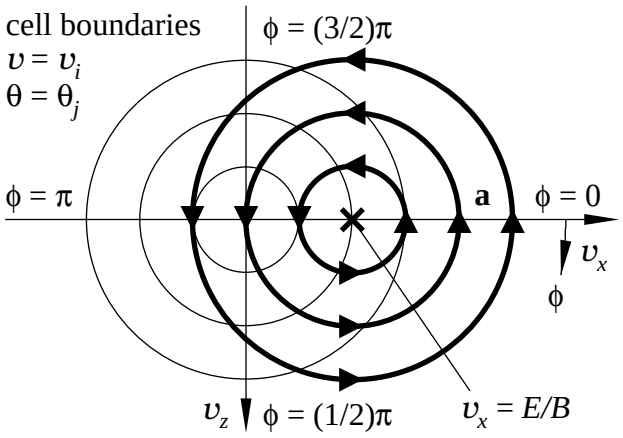

Figure A1. Intersections between the concentric cell boundaries (v- or θ-boundaries) and the acceleration vector $\mathbf{a} = -(e/m)(\mathbf{E}+\mathbf{v}\times\mathbf{B})$. $\mathbf{a}$ crosses the concentric boundaries from the outside to the inside in the region of $v_z < 0$, and from the inside to the outside in the region of $v_z > 0$.

functions by case analysis. The exceptional case that both positive and negative values appear on a boundary may occur on $B^{\phi}_{i,j,k}$. This will be explained in Appendix A.3.

Appendix A.1. Electron flows through v-boundaries

At (v_i, θ, ϕ) on a v-boundary $B^{v}_{i,j,k}$ defined in equation (15), the normal vector $\mathbf{n}^{v}_{i,j,k}$ toward the $+v$ direction and the areal element $\mathrm{d}s^{v}_{i,j,k}$ are

$$\mathbf{n}^{v}_{i,j,k} = (\sin\theta\cos\phi, \cos\theta, \sin\theta\sin\phi), \tag{A.6}$$

$$\mathrm{d}s^{v}_{i,j,k} = v_i^2 \sin\theta\, \mathrm{d}\theta\mathrm{d}\phi. \tag{A.7}$$

Then, $\mathbf{a}\cdot\mathbf{n}^{v}_{i,j,k}\,\mathrm{d}s^{v}_{i,j,k}$ to obtain $K^{\pm v}_{i,j,k}$ in equation (A.3) is

$$\mathbf{a}\cdot\mathbf{n}^{v}_{i,j,k}\,\mathrm{d}s^{v}_{i,j,k} = \omega\frac{E}{B}v_i^2\sin^2\theta\sin\phi\,\mathrm{d}\theta\mathrm{d}\phi. \tag{A.8}$$

The sign of this integrand changes at $\phi = 0$ and π (see figure A1). By letting $k_{\max}$ be an even integer, we can align the borders of the sign change at those between $B^{v}_{i,j,1}$ and $B^{v}_{i,j,k_{\max}}$ and those between $B^{v}_{i,j,k_{\max}/2}$ and $B^{v}_{i,j,k_{\max}/2+1}$. Then, $\mathrm{sgn}(\mathbf{a}\cdot\mathbf{n}^{v}_{i,j,k})$ is unchanged on every $B^{v}_{i,j,k}$.

For $1 \le k \le \frac{1}{2}k_{\max}$ ($0 \le \phi \le \pi$, i.e. $v_z \ge 0$), the direction of the electron flow across $B^{v}_{i,j,k}$ is from $C_{i,j,k}$ to $C_{i+1,j,k}$, i.e. $\mathbf{a}\cdot\mathbf{n}^{v}_{i,j,k} \ge 0$, thus

$$K^{+v}_{i,j,k} = +\frac{1}{4}\omega\frac{E}{B}v_i^2\left[2\Delta\theta - (\sin 2\theta_j - \sin 2\theta_{j-1})\right](\cos\phi_{k-1} - \cos\phi_k), \tag{A.9}$$

$$K^{-v}_{i,j,k} = 0. \tag{A.10}$$

Complementarily, for $\frac{1}{2}k_{\max}+1\le k\le k_{\max}$ ($\pi\le\phi\le 2\pi$, i.e. $v_z\le 0$), the direction of the electron flow across $B^{v}_{i,j,k}$ is from $C_{i+1,j,k}$ to $C_{i,j,k}$, i.e. $\mathbf{a}\cdot\mathbf{n}^{v}_{i,j,k}\le 0$, thus

$$K^{+v}_{i,j,k}=0, \tag{A.11}$$

$$K^{-v}_{i,j,k}=-\frac{1}{4}\omega\frac{E}{B}v_i^2\left[2\Delta\theta-(\sin 2\theta_j-\sin 2\theta_{j-1})\right](\cos\phi_{k-1}-\cos\phi_k). \tag{A.12}$$

Appendix A.2. Electron flows through θ-boundaries

At (v,θ_j,ϕ) on a θ-boundary $B^{\theta}_{i,j,k}$ defined in equation (16), the normal vector $\mathbf{n}^{\theta}_{i,j,k}$ toward the $+\theta$ directions and the areal element $\mathrm{d}s^{\theta}_{i,j,k}$ are

$$\mathbf{n}^{\theta}_{i,j,k}=(\cos\theta_j\cos\phi,-\sin\theta_j,\cos\theta_j\sin\phi), \tag{A.13}$$

$$\mathrm{d}s^{\theta}_{i,j,k}=v\sin\theta_j\,\mathrm{d}v\mathrm{d}\phi. \tag{A.14}$$

Then, $\mathbf{a}\cdot\mathbf{n}^{\theta}_{i,j,k}\,\mathrm{d}s^{\theta}_{i,j,k}$ to obtain $K^{\pm\theta}_{i,j,k}$ in equation (A.4) is

$$\mathbf{a}\cdot\mathbf{n}^{\theta}_{i,j,k}\,\mathrm{d}s^{\theta}_{i,j,k}=\omega\frac{E}{B}v\sin\theta_j\cos\theta_j\sin\phi\,\mathrm{d}v\mathrm{d}\phi=\omega\frac{E}{B}v\frac{\sin 2\theta_j}{2}\sin\phi\,\mathrm{d}v\mathrm{d}\phi. \tag{A.15}$$

The sign of this integrand changes at $\phi=0$ and π (see figure A1). By letting $k_{\max}$ be an even integer, we can align the borders of the sign change at those between $B^{\theta}_{i,j,1}$ and $B^{\theta}_{i,j,k_{\max}}$ and those between $B^{\theta}_{i,j,k_{\max}/2}$ and $B^{\theta}_{i,j,k_{\max}/2+1}$. Then, $\mathrm{sgn}(\mathbf{a}\cdot\mathbf{n}^{\theta}_{i,j,k})$ is unchanged on every $B^{\theta}_{i,j,k}$.

For $1\le k\le\frac{1}{2}k_{\max}$ ($0\le\phi\le\pi$, i.e. $v_z\ge 0$), the direction of the electron flow across $B^{\theta}_{i,j,k}$ is from $C_{i,j,k}$ to $C_{i,j+1,k}$, i.e. $\mathbf{a}\cdot\mathbf{n}^{\theta}_{i,j,k}\ge 0$, thus

$$K^{+\theta}_{i,j,k}=+\frac{1}{4}\omega\frac{E}{B}\left(v_i^2-v_{i-1}^2\right)\sin 2\theta_j(\cos\phi_{k-1}-\cos\phi_k), \tag{A.16}$$

$$K^{-\theta}_{i,j,k}=0. \tag{A.17}$$

Complementarily, for $\frac{1}{2}k_{\max}+1\le k\le k_{\max}$ ($\pi\le\phi\le 2\pi$, i.e. $v_z\le 0$), the direction of the electron flow across $B^{\theta}_{i,j,k}$ is from $C_{i,j+1,k}$ to $C_{i,j,k}$, i.e. $\mathbf{a}\cdot\mathbf{n}^{\theta}_{i,j,k}\le 0$, thus

$$K^{+\theta}_{i,j,k}=0, \tag{A.18}$$

$$K^{-\theta}_{i,j,k}=-\frac{1}{4}\omega\frac{E}{B}\left(v_i^2-v_{i-1}^2\right)\sin 2\theta_j(\cos\phi_{k-1}-\cos\phi_k). \tag{A.19}$$

Appendix A.3. Electron flows through φ-boundaries

At (v,θ,ϕ_k) on a ϕ-boundary $B^{\phi}_{i,j,k}$ defined in equation (17), the normal vector $\mathbf{n}^{\phi}_{i,j,k}$ toward the $+\phi$ direction and the areal element $\mathrm{d}s^{\phi}_{i,j,k}$ are

$$\mathbf{n}^{\phi}_{i,j,k}=(-\sin\phi_k,0,\cos\phi_k), \tag{A.20}$$

$$\mathrm{d}s^{\phi}_{i,j,k}=v\,\mathrm{d}v\mathrm{d}\theta. \tag{A.21}$$

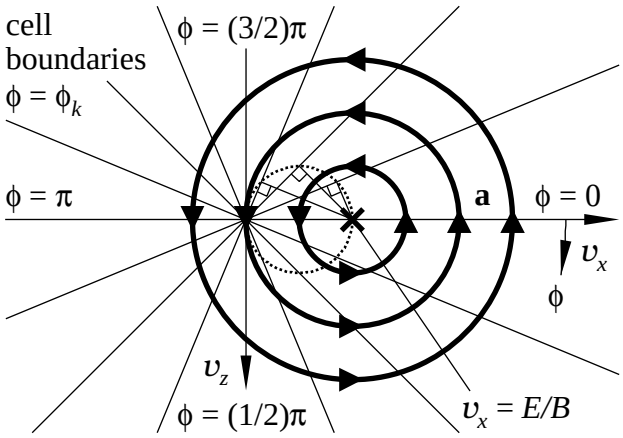

Figure A2. Intersections between the radial cell boundaries (ϕ-boundaries) and the acceleration vector $\mathbf{a} = -(e/m)(\mathbf{E} + \mathbf{v} \times \mathbf{B})$. The dotted circle represents the border at which the crossing direction of $\mathbf{a}$ changes. $\mathbf{a}$ crosses the radial boundaries from the $-\phi$ side to the $+\phi$ side in the dotted circle, and otherwise from the $+\phi$ side to the $-\phi$ side.

Then, $\mathbf{a} \cdot \mathbf{n}^{\phi}_{i,j,k}\, \mathrm{d}s^{\phi}_{i,j,k}$ to obtain $K^{\pm\phi}_{i,j,k}$ in equation (A.5) is

$$\mathbf{a} \cdot \mathbf{n}^{\phi}_{i,j,k}\, \mathrm{d}s^{\phi}_{i,j,k} = -\omega v^2 \sin\theta\, \mathrm{d}v\mathrm{d}\theta + \omega \frac{E}{B} v \cos\phi_k\, \mathrm{d}v\mathrm{d}\theta. \tag{A.22}$$

The sign of the integrand changes at a border $v \sin\theta = (E/B)\cos\phi_k$. Here, $v\sin\theta = \sqrt{v_x^2 + v_z^2}$ ($\equiv v_{xz}$). Because $(E/B)\cos\phi_k$ ($\equiv v_{\mathrm{c}}$) is a constant in the plane of $\phi = \phi_k$ including $B^{\phi}_{i,j,k}$, the border is a line $v_{xz} = v_{\mathrm{c}}$ parallel to the v_y-axis. This border line is the intersection between the plane of $\phi = \phi_k$ and a tubular surface (the side of a cylinder of infinite length) that has an axis $(v_x, v_z) = (\frac{1}{2}(E/B), 0)$ parallel to the v_y-axis and a diameter E/B (see figure A2). The cylinder intersects limited $B^{\phi}_{i,j,k}$ only in the region of $v_x \geq 0$ (i.e. $0 \leq \phi_k \leq \frac{1}{2}\pi$ and $\frac{3}{2}\pi \leq \phi_k \leq 2\pi$). The intersection on $B^{\phi}_{i,j,k}$ is a line $(v_x, v_z) = (v_{\mathrm{c}}\cos\phi_k, v_{\mathrm{c}}\sin\phi_k) = ((E/B)\cos^2\phi_k, (E/B)\cos\phi_k \sin\phi_k)$ parallel to the v_y-axis. Excluding the v_y-axis, that does not divide any $B^{\phi}_{i,j,k}$, the effective intersection between the cylinder and each $B^{\phi}_{i,j,k}$ is at most once in the present cell configuration.

When whole of $B^{\phi}_{i,j,k}$ is in the cylinder, the direction of the electron flow across $B^{\phi}_{i,j,k}$ is from $C_{i,j,k}$ to $C_{i,j,k+1}$, thus

$$K^{+\phi}_{i,j,k} = -\frac{1}{3}\omega \left(v_i^3 - v_{i-1}^3\right)(\cos\theta_{j-1} - \cos\theta_j) + \frac{1}{2}\omega\frac{E}{B}\left(v_i^2 - v_{i-1}^2\right)\Delta\theta\cos\phi_k, \tag{A.23}$$

$$K^{-\phi}_{i,j,k} = 0. \tag{A.24}$$

On the other hand, when whole of $B^{\phi}_{i,j,k}$ is out of the cylinder, the direction of the electron flow across $B^{\phi}_{i,j,k}$ is from $C_{i,j,k+1}$ to $C_{i,j,k}$, thus

$$K^{+\phi}_{i,j,k} = 0, \tag{A.25}$$

$$K^{-\phi}_{i,j,k} = +\frac{1}{3}\omega\left(v_i^3 - v_{i-1}^3\right)\left(\cos\theta_{j-1} - \cos\theta_j\right) - \frac{1}{2}\omega\frac{E}{B}\left(v_i^2 - v_{i-1}^2\right)\Delta\theta\cos\phi_k. \tag{A.26}$$

When $B^{\phi}_{i,j,k}$ has an intersection with the cylinder, the integral domain must be separated into the inside region ($v_{xz} \le v_{\rm c}$) where $K^{+\phi}_{i,j,k} \ge 0$ and $K^{-\phi}_{i,j,k} = 0$, and the outside region ($v_{xz} \ge v_{\rm c}$) where $K^{+\phi}_{i,j,k} = 0$ and $K^{-\phi}_{i,j,k} \ge 0$.

Hereafter, we consider the case that $B^{\phi}_{i,j,k}$ has an intersection with the cylinder. The integrals for $K^{\pm\phi}_{i,j,k}$ can be calculated in the plane of $\phi = \phi_k$ with abscissa v_{xz} and ordinate v_y. The four edges of $B^{\phi}_{i,j,k}$ are numbered as shown in figure A3. They are represented as

edge 1, upper straight line:

$$v_{y,\rm upper}(v_{xz}) = v_{xz}\cot\theta_{j-1}, \tag{A.27}$$

$$v_{xz13} = v_{i-1}\sin\theta_{j-1} \le v_{xz} \le v_{xz12} = v_i\sin\theta_{j-1}, \tag{A.28}$$

edge 2, upper arc:

$$v_{y,\rm upper}(v_{xz}) = \sqrt{v_i^2 - v_{xz}^2}, \tag{A.29}$$

$$v_{xz12} = v_i\sin\theta_{j-1} \le v_{xz} \le v_{xz24} = v_i\sin\theta_j, \tag{A.30}$$

edge 3, lower arc:

$$v_{y,\rm lower}(v_{xz}) = \sqrt{v_{i-1}^2 - v_{xz}^2}, \tag{A.31}$$

$$v_{xz13} = v_{i-1}\sin\theta_{j-1} \le v_{xz} \le v_{xz34} = v_{i-1}\sin\theta_j, \tag{A.32}$$

edge 4, lower straight line:

$$v_{y,\rm lower}(v_{xz}) = v_{xz}\cot\theta_j, \tag{A.33}$$

$$v_{xz34} = v_{i-1}\sin\theta_j \le v_{xz} \le v_{xz24} = v_i\sin\theta_j. \tag{A.34}$$

We assume $v_{xz13} \le v_{\rm c} \le v_{xz24}$. Whether $v_{xz12} < v_{xz34}$ or $v_{xz12} \ge v_{xz34}$ depends on $B^{\phi}_{i,j,k}$.

$\mathbf{a}$ and $\mathbf{n}^{\phi}_{i,j,k}$ are independent of v_y. Thus, in the $v_{xz}v_y$-plane, $\mathbf{a}\cdot\mathbf{n}^{\phi}_{i,j,k}\,\mathrm{d}s^{\phi}_{i,j,k}$ in equation (A.22) can be rewritten by the following $\mathbf{a}\cdot\mathbf{n}^{\phi}_{i,j,k}$ and $\mathrm{d}s^{\phi}_{i,j,k}$ represented with v_{xz} instead of v and θ:

$$\mathbf{a}\cdot\mathbf{n}^{\phi}_{i,j,k} = -\omega v_{xz} + \omega\frac{E}{B}\cos\phi_k, \tag{A.35}$$

$$\mathrm{d}s^{\phi}_{i,j,k} = \left[v_{y,\rm upper}(v_{xz}) - v_{y,\rm lower}(v_{xz})\right]\mathrm{d}v_{xz}. \tag{A.36}$$

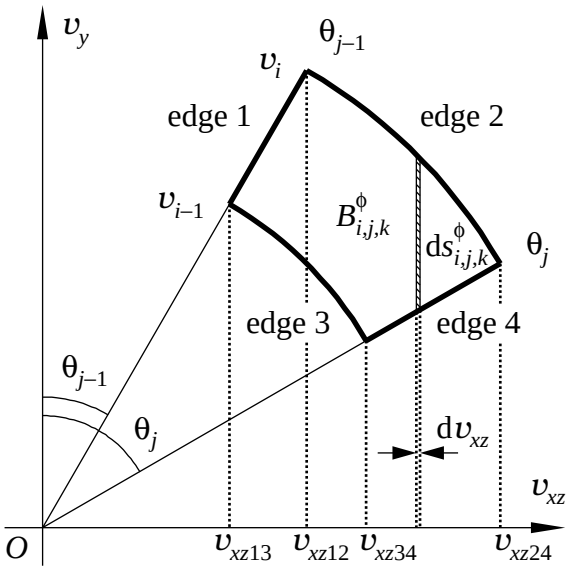

Figure A3. A ϕ-boundary $B^{\phi}_{i,j,k}$ and its areal element $\mathrm{d}s^{\phi}_{i,j,k}$. Because the integrand $\mathbf{a} \cdot \mathbf{n}^{\phi}_{i,j,k}$ is independent of v_y, the areal element can be a strip shape.

Because the direction of the electron flow across $B^{\phi}_{i,j,k}$ is from $C_{i,j,k}$ to $C_{i,j,k+1}$ for $v_{xz} \leq v_{\mathrm{c}}$ and from $C_{i,j,k+1}$ to $C_{i,j,k}$ for $v_{xz} \geq v_{\mathrm{c}}$ as shown in figure A4, $K^{\pm\phi}_{i,j,k}$ are given as

$$\begin{aligned} K^{+\phi}_{i,j,k} &= +\int_{v_{xz13}}^{v_{\mathrm{c}}} \mathbf{a} \cdot \mathbf{n}^{\phi}_{i,j,k} [v_{y,\mathrm{upper}}(v_{xz}) - v_{y,\mathrm{lower}}(v_{xz})] \, \mathrm{d}v_{xz} \\ &= \left(K^{+\phi}_{i,j,k,1} + K^{+\phi}_{i,j,k,2}\right) - \left(K^{+\phi}_{i,j,k,3} + K^{+\phi}_{i,j,k,4}\right), \qquad \text{(A.37)} \\ K^{-\phi}_{i,j,k} &= -\int_{v_{\mathrm{c}}}^{v_{xz24}} \mathbf{a} \cdot \mathbf{n}^{\phi}_{i,j,k} [v_{y,\mathrm{upper}}(v_{xz}) - v_{y,\mathrm{lower}}(v_{xz})] \, \mathrm{d}v_{xz} \\ &= \left(K^{-\phi}_{i,j,k,1} + K^{-\phi}_{i,j,k,2}\right) - \left(K^{-\phi}_{i,j,k,3} + K^{-\phi}_{i,j,k,4}\right), \qquad \text{(A.38)} \\ K^{+\phi}_{i,j,k,1} &= +\int_{v_{xz13}}^{\min(v_{xz12}, v_{\mathrm{c}})} \mathbf{a} \cdot \mathbf{n}^{\phi}_{i,j,k} v_{y,\mathrm{upper}}(v_{xz}) \, \mathrm{d}v_{xz}, \qquad \text{(A.39)} \\ K^{-\phi}_{i,j,k,1} &= -\int_{\min(v_{xz12}, v_{\mathrm{c}})}^{v_{xz12}} \mathbf{a} \cdot \mathbf{n}^{\phi}_{i,j,k} v_{y,\mathrm{upper}}(v_{xz}) \, \mathrm{d}v_{xz}, \qquad \text{(A.40)} \\ K^{+\phi}_{i,j,k,2} &= +\int_{v_{xz12}}^{\max(v_{xz12}, v_{\mathrm{c}})} \mathbf{a} \cdot \mathbf{n}^{\phi}_{i,j,k} v_{y,\mathrm{upper}}(v_{xz}) \, \mathrm{d}v_{xz}, \qquad \text{(A.41)} \\ K^{-\phi}_{i,j,k,2} &= -\int_{\max(v_{xz12}, v_{\mathrm{c}})}^{v_{xz24}} \mathbf{a} \cdot \mathbf{n}^{\phi}_{i,j,k} v_{y,\mathrm{upper}}(v_{xz}) \, \mathrm{d}v_{xz}, \qquad \text{(A.42)} \\ K^{+\phi}_{i,j,k,3} &= +\int_{v_{xz13}}^{\min(v_{xz34}, v_{\mathrm{c}})} \mathbf{a} \cdot \mathbf{n}^{\phi}_{i,j,k} v_{y,\mathrm{lower}}(v_{xz}) \, \mathrm{d}v_{xz}, \qquad \text{(A.43)} \\ K^{-\phi}_{i,j,k,3} &= -\int_{\min(v_{xz34}, v_{\mathrm{c}})}^{v_{xz34}} \mathbf{a} \cdot \mathbf{n}^{\phi}_{i,j,k} v_{y,\mathrm{lower}}(v_{xz}) \, \mathrm{d}v_{xz}, \qquad \text{(A.44)} \\ K^{+\phi}_{i,j,k,4} &= +\int_{v_{xz34}}^{\max(v_{xz34}, v_{\mathrm{c}})} \mathbf{a} \cdot \mathbf{n}^{\phi}_{i,j,k} v_{y,\mathrm{lower}}(v_{xz}) \, \mathrm{d}v_{xz}, \qquad \text{(A.45)} \end{aligned}$$

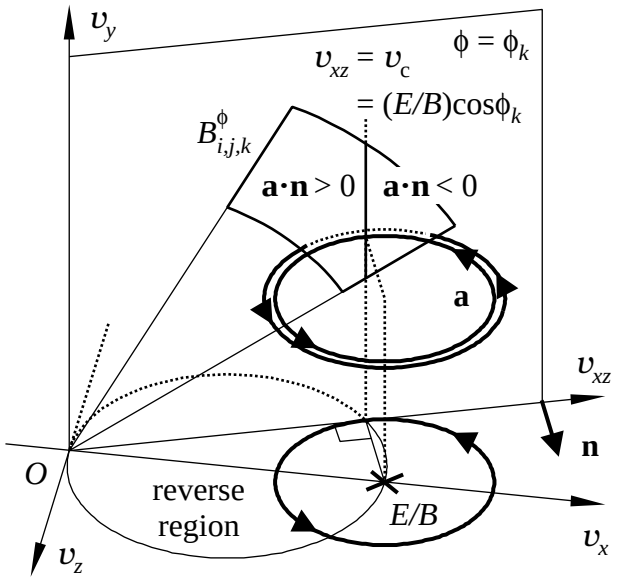

Figure A4. A ϕ-boundary $B^{\phi}_{i,j,k}$ having the border $v_{xz} = v_c = (E/B)\cos\phi_k$, at which $\mathrm{sgn}(\mathbf{a}\cdot\mathbf{n})$ changes. The electron flow across such a boundary is mutual between the two cells contacting at $B^{\phi}_{i,j,k}$.

$$K^{-\phi}_{i,j,k,4} = -\int_{\max(v_{xz34}, v_c)}^{v_{xz24}} \mathbf{a}\cdot\mathbf{n}^{\phi}_{i,j,k} v_{y,\mathrm{lower}}(v_{xz})\,\mathrm{d}v_{xz}. \tag{A.46}$$

In order to calculate these eight terms, let us introduce parameters v_L and v_U to represent an integral domain $v_\mathrm{L} \le v_{xz} \le v_\mathrm{U}$ in which $\mathrm{sgn}(\mathbf{a}\cdot\mathbf{n}^{\phi}_{i,j,k})$ is unchanged. In the following subsections, the integrals for $K^{\pm\phi}_{i,j,k,l}$ (l = 1–4) in equations (A.39)–(A.46) are calculated using v_L and v_U. After that, practical values of v_L and v_U are chosen depending on whether $v_{xz12} \ge v_c$ or $v_{xz12} < v_c$ and whether $v_{xz34} \ge v_c$ or $v_{xz34} < v_c$.

Appendix A.3.1. Integral along edge 1: upper straight line $K^{\pm\phi}_{i,j,k,1}$ in equations (A.39) and (A.40) are given as follows by introducing an integral $K_1(v_\mathrm{L}, v_\mathrm{U})$ along edge 1 in equation (A.27):

$$K^{+\phi}_{i,j,k,1} = +K_1(v_{xz13}, \min(v_{xz12}, v_c)), \tag{A.47}$$

$$K^{-\phi}_{i,j,k,1} = -K_1(\min(v_{xz12}, v_c), v_{xz12}), \tag{A.48}$$

$$\begin{aligned} K_1(v_\mathrm{L}, v_\mathrm{U}) &= \int_{v_\mathrm{L}}^{v_\mathrm{U}} \mathbf{a}\cdot\mathbf{n}^{\phi}_{i,j,k} v_{y,\mathrm{upper}}(v_{xz})\,\mathrm{d}v_{xz} \\ &= \int_{v_\mathrm{L}}^{v_\mathrm{U}} \left(-\omega v_{xz}^2 \cot\theta_{j-1} + \omega\frac{E}{B} v_{xz}\cot\theta_{j-1}\cos\phi_k\right)\mathrm{d}v_{xz} \\ &= -\frac{1}{3}\omega\left(v_\mathrm{U}^3 - v_\mathrm{L}^3\right)\cot\theta_{j-1} + \frac{1}{2}\omega\frac{E}{B}\left(v_\mathrm{U}^2 - v_\mathrm{L}^2\right)\cot\theta_{j-1}\cos\phi_k. \end{aligned} \tag{A.49}$$

When the integral domain covers all of the v_{xz} range of edge 1,

$$\begin{aligned} K_1^{\text{full}} &= K_1(v_{xz13}=v_{i-1}\sin\theta_{j-1}, v_{xz12}=v_i\sin\theta_{j-1}) \\ &= -\frac{1}{3}\omega\left(v_i^3-v_{i-1}^3\right)\cos\theta_{j-1}\sin^2\theta_{j-1} \\ &\quad + \frac{1}{2}\omega\frac{E}{B}\left(v_i^2-v_{i-1}^2\right)\cos\theta_{j-1}\sin\theta_{j-1}\cos\phi_k. \end{aligned} \tag{A.50}$$

Appendix A.3.2. Integral along edge 2: upper arc $K_{i,j,k,2}^{\pm\phi}$ in equations (A.41) and (A.42) are given as follows by introducing an integral $K_2(v_{\mathrm{L}}, v_{\mathrm{U}})$ along edge 2 in equation (A.29):

$$K_{i,j,k,2}^{+\phi} = +K_2(v_{xz12}, \max(v_{xz12}, v_{\mathrm{c}})), \tag{A.51}$$

$$K_{i,j,k,2}^{-\phi} = -K_2(\max(v_{xz12}, v_{\mathrm{c}}), v_{xz24}), \tag{A.52}$$

$$\begin{aligned} K_2(v_{\mathrm{L}}, v_{\mathrm{U}}) &= \int_{v_{\mathrm{L}}}^{v_{\mathrm{U}}} \mathbf{a}\cdot\mathbf{n}_{i,j,k}^{\phi} v_{y,\mathrm{upper}}(v_{xz})\,\mathrm{d}v_{xz} \\ &= -\int_{v_{\mathrm{L}}}^{v_{\mathrm{U}}} \omega v_{xz}\sqrt{v_i^2-v_{xz}^2}\,\mathrm{d}v_{xz} + \int_{v_{\mathrm{L}}}^{v_{\mathrm{U}}} \omega\frac{E}{B}\sqrt{v_i^2-v_{xz}^2}\cos\phi_k\,\mathrm{d}v_{xz}. \end{aligned} \tag{A.53}$$

The first term in the right-hand side of equation (A.53) becomes

$$\begin{aligned} -\int_{v_{\mathrm{L}}}^{v_{\mathrm{U}}} \omega v_{xz}\sqrt{v_i^2-v_{xz}^2}\,\mathrm{d}v_{xz} &= -\omega\left[\frac{2}{3}\left(-\frac{1}{2}\right)\left(v_i^2-v_{xz}^2\right)^{3/2}\right]_{v_{\mathrm{L}}}^{v_{\mathrm{U}}} \\ &= \frac{1}{3}\omega\left[\left(v_i^2-v_{\mathrm{U}}^2\right)^{3/2} - \left(v_i^2-v_{\mathrm{L}}^2\right)^{3/2}\right]. \end{aligned} \tag{A.54}$$

The second term in the right-hand side of equation (A.53) becomes

$$\begin{aligned} \int_{v_{\mathrm{L}}}^{v_{\mathrm{U}}} \omega\frac{E}{B}\sqrt{v_i^2-v_{xz}^2}\cos\phi_k\,\mathrm{d}v_{xz} &= \int_{\theta_{\mathrm{L}}}^{\theta_{\mathrm{U}}} \omega\frac{E}{B}v_i^2\cos^2\theta\cos\phi_k\,\mathrm{d}\theta \\ &= \int_{\theta_{\mathrm{L}}}^{\theta_{\mathrm{U}}} \omega\frac{E}{B}v_i^2\frac{1+\cos 2\theta}{2}\cos\phi_k\,\mathrm{d}\theta \\ &= \omega\frac{E}{B}v_i^2\left[\frac{1}{2}\theta+\frac{1}{4}\sin 2\theta\right]_{\theta_{\mathrm{L}}}^{\theta_{\mathrm{U}}}\cos\phi_k \\ &= \omega\frac{E}{B}v_i^2\left[\frac{1}{2}(\theta_{\mathrm{U}}-\theta_{\mathrm{L}})+\frac{1}{4}(\sin 2\theta_{\mathrm{U}}-\sin 2\theta_{\mathrm{L}})\right]\cos\phi_k. \end{aligned} \tag{A.55}$$

Here, the integral variable was converted into θ by relations $v_{xz} = v_i\sin\theta$, $\mathrm{d}v_{xz} = v_i\cos\theta\,\mathrm{d}\theta$, $\theta_{\mathrm{L}} = \sin^{-1}(v_{\mathrm{L}}/v_i)$ and $\theta_{\mathrm{U}} = \sin^{-1}(v_{\mathrm{U}}/v_i)$. From equations (A.54) and (A.55), equation (A.53) becomes

$$\begin{aligned} K_2(v_{\mathrm{L}}, v_{\mathrm{U}}) &= \frac{1}{3}\omega\left[\left(v_i^2-v_{\mathrm{U}}^2\right)^{3/2} - \left(v_i^2-v_{\mathrm{L}}^2\right)^{3/2}\right] \\ &\quad + \omega\frac{E}{B}v_i^2\left[\frac{1}{2}(\theta_{\mathrm{U}}-\theta_{\mathrm{L}})+\frac{1}{4}(\sin 2\theta_{\mathrm{U}}-\sin 2\theta_{\mathrm{L}})\right]\cos\phi_k. \end{aligned} \tag{A.56}$$

When the integral domain covers all of the v_{xz} range of edge 2,

$$\begin{aligned} K_2^{\text{full}} &= K_2(v_{xz12}=v_i\sin\theta_{j-1}, v_{xz24}=v_i\sin\theta_j) \\ &= \frac{1}{3}\omega v_i^3\left(\cos^3\theta_j-\cos^3\theta_{j-1}\right) \\ &\quad + \omega\frac{E}{B}v_i^2\left[\frac{1}{2}\Delta\theta+\frac{1}{4}(\sin 2\theta_j-\sin 2\theta_{j-1})\right]\cos\phi_k. \end{aligned} \tag{A.57}$$

Appendix A.3.3. Integral along edge 3: lower arc $K_{i,j,k,3}^{\pm\phi}$ in equations (A.43) and (A.44) are given as follows by introducing an integral $K_3(v_{\text{L}},v_{\text{U}})$ along edge 3 in equation (A.31):

$$K_{i,j,k,3}^{+\phi} = +K_3(v_{xz13},\min(v_{xz34},v_{\text{c}})), \tag{A.58}$$

$$K_{i,j,k,3}^{-\phi} = -K_3(\min(v_{xz34},v_{\text{c}}),v_{xz34}), \tag{A.59}$$

$$\begin{aligned} K_3(v_{\text{L}},v_{\text{U}}) &= \int_{v_{\text{L}}}^{v_{\text{U}}}\mathbf{a}\cdot\mathbf{n}_{i,j,k}^{\phi}v_{y,\text{lower}}(v_{xz})\,\mathrm{d}v_{xz} \\ &= -\int_{v_{\text{L}}}^{v_{\text{U}}}\omega v_{xz}\sqrt{v_{i-1}^2-v_{xz}^2}\,\mathrm{d}v_{xz}+\int_{v_{\text{L}}}^{v_{\text{U}}}\omega\frac{E}{B}\sqrt{v_{i-1}^2-v_{xz}^2}\cos\phi_k\,\mathrm{d}v_{xz}. \end{aligned} \tag{A.60}$$

From a comparison between equations (A.53) and (A.60), $K_3(v_{\text{L}},v_{\text{U}})$ is obtained by replacing v_i in equation (A.56) with v_{i-1}:

$$\begin{aligned} K_3(v_{\text{L}},v_{\text{U}}) &= \frac{1}{3}\omega\left[\left(v_{i-1}^2-v_{\text{U}}^2\right)^{3/2}-\left(v_{i-1}^2-v_{\text{L}}^2\right)^{3/2}\right] \\ &\quad + \omega\frac{E}{B}v_{i-1}^2\left[\frac{1}{2}(\theta_{\text{U}}-\theta_{\text{L}})+\frac{1}{4}(\sin 2\theta_{\text{U}}-\sin 2\theta_{\text{L}})\right]\cos\phi_k. \end{aligned} \tag{A.61}$$

When the integral domain covers all of the v_{xz} range of edge 3,

$$\begin{aligned} K_3^{\text{full}} &= K_3(v_{xz13}=v_{i-1}\sin\theta_{j-1}, v_{xz34}=v_{i-1}\sin\theta_j) \\ &= \frac{1}{3}\omega v_{i-1}^3\left(\cos^3\theta_j-\cos^3\theta_{j-1}\right) \\ &\quad + \omega\frac{E}{B}v_{i-1}^2\left[\frac{1}{2}\Delta\theta+\frac{1}{4}(\sin 2\theta_j-\sin 2\theta_{j-1})\right]\cos\phi_k. \end{aligned} \tag{A.62}$$

Appendix A.3.4. Integral along edge 4: lower straight line $K_{i,j,k,4}^{\pm\phi}$ in equations (A.45) and (A.46) are given as follows by introducing an integral $K_4(v_{\text{L}},v_{\text{U}})$ along edge 4 in equation (A.33):

$$K_{i,j,k,4}^{+\phi} = +K_4(v_{xz34},\max(v_{xz34},v_{\text{c}})), \tag{A.63}$$

$$K_{i,j,k,4}^{-\phi} = -K_4(\max(v_{xz34},v_{\text{c}}),v_{xz24}), \tag{A.64}$$

$$\begin{aligned} K_4(v_{\text{L}},v_{\text{U}}) &= \int_{v_{\text{L}}}^{v_{\text{U}}}\mathbf{a}\cdot\mathbf{n}_{i,j,k}^{\phi}v_{y,\text{lower}}(v_{xz})\,\mathrm{d}v_{xz} \\ &= \int_{v_{\text{L}}}^{v_{\text{U}}}\left(-\omega v_{xz}^2\cot\theta_j+\omega\frac{E}{B}v_{xz}\cot\theta_j\cos\phi_k\right)\mathrm{d}v_{xz} \\ &= -\frac{1}{3}\omega\left(v_{\text{U}}^3-v_{\text{L}}^3\right)\cot\theta_j+\frac{1}{2}\omega\frac{E}{B}\left(v_{\text{U}}^2-v_{\text{L}}^2\right)\cot\theta_j\cos\phi_k. \end{aligned} \tag{A.65}$$

When the integral domain covers all of the v_{xz} range of edge 4,

$$\begin{aligned} K_4^{\text{full}} &= K_4(v_{xz34} = v_{i-1}\sin\theta_j, v_{xz24} = v_i \sin\theta_j) \\ &= -\frac{1}{3}\omega\left(v_i^3 - v_{i-1}^3\right)\cos\theta_j \sin^2\theta_j \\ &\quad + \frac{1}{2}\omega\frac{E}{B}\left(v_i^2 - v_{i-1}^2\right)\cos\theta_j \sin\theta_j \cos\phi_k. \end{aligned} \tag{A.66}$$

References

[1] Holstein T 1946 *Phys. Rev.* **70** 367–84

[2] Kumar K, Skullerud H R and Robson R E 1980 *Aust. J. Phys.* **33** 343–448

[3] Yachi S, Kitamura Y, Kitamori K and Tagashira H 1988 *J. Phys. D: Appl. Phys.* **21** 914–21

[4] Yachi S, Date H, Kitamori K and Tagashira H 1991 *J. Phys. D: Appl. Phys.* **24** 573–80

[5] Boyle G J, Tattersall W J, Cocks D G, Dujko S and White R D 2015 *Phys. Rev.* A**91** 052710

[6] Boyle G J, McEachran R P, Cocks D G and White R D 2015 *J. Chem. Phys.* **142** 154507

[7] Boyle G J, McEachran R P, Cocks D G, Brunger M J, Buckman S J, Dujko S and White R D 2016 *J. Phys. D: Appl. Phys.* **49** 355201

[8] Drallos P J and Wadehra J M 1988 *J. Appl. Phys.* **63** 5601–3

[9] Drallos P J and Wadehra J M 1989 *Phys. Rev. A* **40** 1967–75

[10] Sommerer T J, Hitchon W N G, Harvey R E P and Lawler J E 1991 *Phys. Rev. A* **43** 4452–72

[11] Maeda K and Makabe T 1994 *Japan. J. Appl. Phys.* **33** 4173–6

[12] Shimada T, Nakamura Y, Petrović Z Lj and Makabe T 2003 *J. Phys. D: Appl. Phys.* **36** 1936–46

[13] Sugawara H and Sakai Y 2003 *J. Phys. D: Appl. Phys.* **36** 1994–2000

[14] Sommerer T J, Hitchon W N G and Lawler J E 1989 *Phys. Rev. A* **39** 6356–66

[15] Sugawara H, Sakai Y and Tagashira H 1992 *J. Phys. D: Appl. Phys.* **25** 1483–7

[16] Sugawara H, Sakai Y and Tagashira H 1994 *J. Phys. D: Appl. Phys.* **27** 90–4

[17] Sugawara H, Sakai Y and Tagashira H 1995 *J. Phys. D: Appl. Phys.* **28** 61–7

[18] Sugawara H, Tagashira H and Sakai Y 1997 *J. Phys. D: Appl. Phys.* **30** 368–73

[19] Sugawara H, Sakai Y, Tagashira H and Kitamori K 1998 *J. Phys. D: Appl. Phys.* **31** 319–27

[20] Sugawara H and Sakai Y 1999 *J. Phys. D: Appl. Phys.* **32** 1671–80

[21] Sugawara H and Sakai Y 2006 *Japan. J. Appl. Phys.* **45** 5189–96

[22] Hitchon W N G, Koch D J and Adams J B 1989 *J. Comput. Phys.* **83** 79–95

[23] Tan W, Hoekstra R J and Kushner M J 1996 *J. Appl. Phys.* **79** 3423–31

[24] Christlieb A J, Hitchon W N G, Lawler J E and Lister G G 2009 *J. Phys. D: Appl. Phys.* **42** 194007

[25] Wichaidit C, Hitchon W N G, Lawler J E and Lister G G 2009 *J. Phys. D: Appl. Phys.* **42** 025202

[26] Golubovskii Y B, Porokhova I A, Lange H, Gortchakov S and Uhrlandt D 2005 *Plasma Sources Sci. Technol.* **14** 45–50

[27] Golubovskii Y, Gorchakov S and Uhrlandt D 2013 *Plasma Sources Sci. Technol.* **22** 023001

[28] Fixel D A and Hitchon W N G 2007 J. Comput. Phys. **227** 1387–410

[29] Sugawara H 2017 *Plasma Sources Sci. Technol.* **26** 044002

[30] Sugawara H 2019 *IEEE Trans. Plasma Sci.* **47** 1071–82

[31] Sugawara H 2017 *Proc. 10th Asia-Pacific Int. Symp. Basics and Applications of Plasma Technol. (Taoyuan, Taiwan, 15-17 December)* S3-01

[32] Sugawara H and Matsumoto S 2017 *National Convention Record, Institute of Electrical Engineers of Japan (Toyama, Japan, 15–17 March)* No. 1-066 [in Japanese]

[33] Sugawara H 2017 *Proc. 33rd Int. Conf. Phenomena in Ionized Gases (Estoril, Portugal, 9–14 July)*

PI.6

[34] Sugawara H 2018 *Proc. 19th Asian Conf. on Electrical Discharge (Xianyang, Shaanxi, China, 24–28 November)* I-1

[35] Uchida T 1998 *J. Vac. Sci. Technol. A* **16** 1529–36

[36] Uchida T and Hamaguchi S 2008 *J. Phys. D: Appl. Phys.* **41** 083001

[37] O'Connell D, Gans T, Crintea D L, Czarnetzki U and Sadeghi N 2008 *Plasma Sources Sci. Technol.* **17** 024022

[38] Sugawara H, Osaga T, Tsuboi H, Kuwahara K and Ogata S 2010 *Japan. J. Appl. Phys.* **49** 086001

[39] Osaga T, Sugawara H and Sakurai Y 2011 *Plasma Sources Sci. Technol.* **20** 065003

[40] Tsankov T and Czarnetzki U 2011 AIP Conf. Proc. **1390** 140–9

[41] Celik Y, Tsankov T and Czarnetzki U 2011 *IEEE Trans. Plasma Sci.* **39** 2466–7

[42] Tsankov T and Czarnetzki U 2011 *IEEE Trans. Plasma Sci.* **39** 2538–9

[43] Tsankov T V, Toko K and Czarnetzki U 2012 *Phys. Plasmas* **19** 123503

[44] Sugawara H and Ogino S 2016 *Japan. J. Appl. Phys.* **55** 07LD05

[45] Sugawara H, Yahata T, Oda A and Sakai Y 2000 *J. Phys. D: Appl. Phys.* **33** 1191–6

[46] Reid I D 1979 *Aust. J. Phys.* **32** 231–54

[47] Itoh H, Miura Y, Ikuta N, Nakao Y and Tagashira H 1988 *J. Phys. D: Appl. Phys.* **21** 922–30

[48] Itoh H, Matsumura T, Satoh K, Date H, Nakao Y and Tagashira H 1993 *J. Phys. D: Appl. Phys.* **26** 1975–9

[49] Ness K F 1994 *J. Phys. D: Appl. Phys.* **27** 1848–61

[50] White R D, Brennan M J and Ness K F 1997 *J. Phys. D: Appl. Phys.* **30** 810–6

[51] Sugawara H 2018 *Japan. J. Appl. Phys.* **57** 038001

[52] Kitamori K, Tagashira H and Sakai Y 1980 *J. Phys. D: Appl. Phys.* **13** 535–50

[53] Raspopović Z, Sakadžić S, Petrović Z Lj and Makabe T 2000 *J. Phys. D: Appl. Phys.* **33** 1298–302

[54] White R D, Ness K F and Robson R E 2002 *Appl. Surf. Sci.* **192** 26–49

[55] Dujko S, White R D, Petrović Z Lj and Robson R E 2011 *Plasma Sources Sci. Technol.* **20** 024013

[56] White R D, Ness K F, Robson R E and Li B 1999 *Phys. Rev. E* **60** 2231–49

[57] Dujko S, White R D, Ness K F, Petrović Z Lj and Robson R E 2006 *J. Phys. D: Appl. Phys.* **39** 4788–98

[58] Dujko S, White R D, Petrović Z Lj and Robson R E 2010 *Phys. Rev. E* **81** 046403